



SINTEF

excon

Grønn forvaltning av konstruksjoner for infrastruktur

Kilde: Votna I, Jan Lindgård, SINTEF

Report

State-of-the-art report – NLFEA of deteriorated concrete structures

[Klikk eller trykk her for å skrive inn tekst.]

Author(s):

Reignard Tan, Katarzyna Ostapska, Ruben Løland Sælen, Max Milan Loo, Jelena Zivkovic, Cosmin Popescu, Dan Isdahl-Engh, Kjell Tore Fosså, Kathrine Mürer Stemland, Jan Lindgård, Simen Kongshaug, Kåre Reknes

Report No:

2024:01542 - Unrestricted

Client(s) (pos partner):

SINTEF AS

Report

State-of-the-art report – NLFEA of deteriorated concrete structures

[Klikk eller trykk her for å skrive inn tekst.]

KEYWORDS

Klikk eller trykk her for
å skrive inn tekst.

VERSION

2

DATE

2024-12-17

MAIN AUTHOR(S)

Reignard Tan, Katarzyna Ostapska, Ruben Løland Sælen, Max Milan Loo, Jelena Zivkovic, Cosmin Popescu, Dan Isdahl-Eng, Kjell Tore Fosså, Kathrine Mürer Stemland, Jan Lindgård, Simen Kongshaug, Kåre Reknes

CLIENT(S)

SINTEF AS

CLIENT'S REFERENCE

Tor Arne Hammer

PROJECT NO.

102028198

NO. OF PAGES

62

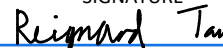
SUMMARY

State-of-the-art report for performing nonlinear finite element analysis to assess the structural integrity of deteriorated reinforced concrete structures. In accordance with the scope and objects set out in work package H3.5.

PREPARED BY

Reignard Tan

SIGNATURE



Reignard Tan (24. feb.. 2025 13:53 GMT+1)

CHECKED BY

Rune Nilsen

SIGNATURE

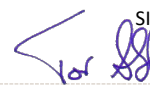


Rune Nilsen (24. feb.. 2025 15:14 GMT+1)

APPROVED BY

Tor Arne Martius-Hammer

SIGNATURE



REPORT NO.

2024:01542

ISBN

978-82-14-07250-1

CLASSIFICATION

Unrestricted

CLASSIFICATION THIS PAGE

Unrestricted

Document history

VERSION	DATE	VERSION DESCRIPTION
1	2023-12-15	
2	2024-12-17	

Preface

This report is part of a series of State-of-the reports (STAR) written for the R&D project EXCON – Sustainable management guidelines to extend the service life of concrete constructions and infrastructure. The current STAR report is a milestone within work package 3 (condition assessment), task 5 (Non-linear Finite Element Analysis of deteriorated concrete structures).

The report summarizes the state-of-the-art for assessing concrete structures subjected to deterioration caused by reinforcement corrosion and alkali silica reactions using nonlinear finite element analysis. The report was written with significant contributions from project partners.

The project is financed by Green Platform agreement being a collaboration between the Norwegian Research Council, Innovation Norway, Siva and Enova. The following partners are involved in the research project.

Infrastructure owners: Equinor (representing offshore platforms), Glitre Energi, Hafslund Eco, Hydro, SFE (all representing dams), Nordland County Municipality and Norwegian Public Roads Administration (both representing bridges)

Consulting agencies: Multiconsult, Norconsult, OPAK

Executing companies: Aker Solutions, Protector

Method suppliers: Consolvo, Elop

Material suppliers: Mapei

Digitalisation: ProXpect drones

R&D: SINTEF, NTNU

Table of contents

1	Introduction	6
1.1	General.....	6
1.2	Scope.....	6
1.3	Advanced structural analysis in Excon	6
2	Challenges and approaches	7
3	Advanced monitoring - Leveraging State-of-the-Art Technologies for Structural Integrity Evaluation	8
3.1	General.....	8
3.1.1	Drones: Unveiling Structures from Above	8
3.1.2	LiDAR: 3D Reconstruction and Defect Detection	8
3.1.3	Hyperspectral Imagery: Spectral Analysis for Defect Identification.....	9
3.1.4	Photogrammetry: 3D Modeling and Visualization	9
3.1.5	Handheld Ultrasound Scanners: Non-Destructive Evaluation.....	9
3.1.6	Integrating Advanced Technologies for Comprehensive Monitoring	9
3.2	Robot and drones.....	9
3.3	Advanced data handling and processing	10
3.4	Detection of cracks and crack patterns.....	11
3.4.1	Photogrammetry	11
3.4.2	Case Studies Demonstrating Photogrammetry's Effectiveness	12
4	Damage mechanisms	12
4.1	Exposure, deterioration, and durability	12
4.1.1	Exposure conditions	12
4.1.2	Permeability.....	12
4.1.3	Diffusion.....	13
4.1.4	Chloride diffusion coefficient in cracked concrete.....	14
4.1.5	Mechanical Property development.....	15
4.2	Reinforcement corrosion	16
4.3	Prestressing damages	17
4.4	Alkali Silika Reaction	17
4.4.1	Reaction process.....	17
4.4.2	Damage mechanisms.....	18
5	Numerical modelling	23
5.1	General.....	23
5.1.1	Systematic literature search	23

5.1.2	Pioneering work identified via cross-referencing of recent literature:.....	25
5.2	NLFEA of concrete structures.....	26
5.2.1	General	26
5.2.2	Material modelling of concrete	27
5.2.3	Material modelling of reinforcing steel	40
5.2.4	Material modelling of prestressing steel	41
5.2.5	Modelling of tension stiffening.....	41
5.3	Modelling of reinforcement corrosion.....	42
5.3.1	General	42
5.3.2	Pitting corrosion	43
5.3.3	Uniform corrosion	45
5.4	Modelling of damaged prestressing	45
5.5	Modelling of ASR.....	45
5.5.1	Introduction: Material characteristics of ASR-affected concrete, and structural consequences	45
5.5.2	Modelling ASR-induced expansions.....	47
5.5.3	Modelling material degradation.....	49
5.5.4	Modelling reinforced concrete structures affected by ASR—important aspects and challenges.	50
5.6	Safety format	51
6	Conclusion	53
7	Future research	53
8	References	54

APPENDICES

Klikk eller trykk her for å skrive inn tekst.

1 Introduction

1.1 General

Excon aims to develop methods for minimizing the use of destructive test methods, work, and related cost during service life survey of structures. The main purpose is to increase knowledge regarding new technology instead of traditional maintenance methods, such as use of non-destructive test methods (NDT), robot and drones, advanced data handling and processing, and advanced structural analysis based on nonlinear finite element analysis (NLFEA). This state-of-the-art report (STAR) will in specific focus on how advanced structural analysis using NLFEA can be applied for such purposes. The aim is to use this report as basis to develop a framework that can assess both the *current state* of a structure and the *future behaviour*. This enables the possibility of performing just-in-time maintenance with specific measures instead of traditional maintenance with pre-determined time intervals.

1.2 Scope

NLFEA for assessing the behaviour of concrete structures realistically has been applied for several decades, and there exists several approaches for modelling the composite material behaviour of concrete and reinforcing and prestressing steel as discussed in chapter 5. This STAR will not focus on the material modelling, but rather on a generic approach for performing NLFEA to assess the structural integrity of deteriorated concrete structures. Hence, the scope set out in this project is to provide guidelines on the following topics:

- Composition of material models consistent with one another
- Deterioration caused by corrosion in reinforcing and prestressing steel
- Deterioration caused by Alkali Silika Reaction (ASR)
- Safety format

This document reports the latest state-of-the-art related to these topics, which will form the basis for the point of depart in the project. The STAR will also from a conceptual perspective address the relevant deterioration mechanisms, and how the use of NDT, robot and drones and advanced data handling and processing will be paramount to serve necessary input to the finite element (FE) models.

1.3 Advanced structural analysis in Excon

The most effective way to reduce greenhouse gas emissions is to extend the service life and use of the existing structures. The alternative is to demolish and build a new structure when the end of service life has been reached. Structures for infrastructure are exposed to aggressive environments and are difficult to access for maintenance. The cost and greenhouse gas emissions relating to demolishing and building new are substantial.

Cost-benefit is usually the single most important factor that determines the choice of management strategy to maintain the performance and purpose that the structure is designed for. The environmental performance, especially the global warming potential (GWP), is an at least equally important factor, and not only as an environmental requirement, but also as a cost contribution due to CO₂ tax and EU's taxonomy. This complicates the choice of management strategy.

The load capacity of an undamaged structure can be calculated using traditional methods. The condition of the structure is investigated and described during service life survey. The quality of the inspection done during the service life survey is crucial input to assess and describe the need for maintenance and repair, and to estimate the structure's load capacity. Lifetime models are used to estimate the remaining lifetime of the structure. Lifetime models must be calibrated against real performance, and against the calculated real safety/load capacity of the structure.

Analysis made with advanced calculation tools show that actual capacity can be significantly greater than originally calculated (Bagge, Popescu, & Elfgren, 2017). Such advanced calculations can also be used to verify capacity and duration of service life. Reliable models that consider the consequences of degradation on the structure's capacity and thus safety, is lacking.

Advanced structural analysis provides an efficient method to study the response of quite complex and large reinforced concrete structures taking into consideration as-built structural details as well as changes in loading and materials during the service life of the structures. Comparisons between numerical results and observations, indicate that an accurate knowledge of the as-built structural details and conservation, may permit pointing out potential criticalities and analyse the robustness of existing structures to avoid the premature end of their life (N. Scattarreggia, 2023).

Advanced structural analysis (NLFEA) is based on theoretical and experimental studies developing statistical models, which are combined with advanced structural analysis to derive reliability-based acceptance criteria for robustness, durability, and functionality. The framework for NLFEA, that is to be developed, will form the basis for modelling existing structures with damage and repairs. In other words, inspection- and maintenance routines provide an overview of the damages to a structure, but only NLFEA can use that information to provide realistic assessments of the structural integrity.

2 Challenges and approaches

Nonlinear finite element analyses (NLFEA) can provide more accurate results than traditional linear analyses (LFEA), but at the cost of increased complexity and the need for careful judgement from the analyst – both in the modelling and in the interpretation of the results.

One immediate difference between NLFEA and LFEA is in the material modelling. To obtain accurate results for concrete structures with NLFEA, the nonlinear behaviour of concrete needs to be modelled. Material models for concrete are typically quite complex to take into account effects such as pressure sensitivity, compaction, crushing and cracking. If the analyst is not familiar with the material model at hand, the choice of material parameters in the analysis might lead to non-conservative results. Another challenge when it comes to material modelling of concrete is the length scale of the problem. On a material level concrete is a brittle material, but on a structural level it exhibits ductile behaviour. If a material model intended for local analyses with element sizes on the mm-scale is used in structural analyses with elements on the cm-scale, the ductility of the structure will be underestimated and could lead to unreasonable non-conservative results. Care must thus be taken to choose a material model appropriate for the analysis in question.

Another challenge in NLFEA comes from the chosen solution technique. Static problems are typically analysed with an implicit solution method where prescribed loads/displacements are applied to the structure in increments and Newton-Raphson iterations are performed to achieve equilibrium for each increment. The relatively large increments in implicit analyses make the solution method unsuitable for problems with rapid changes in stiffness, such as cracking and crushing of concrete in analyses with nonlinear material models. Load controlled implicit analyses are unable to trace post-failure response of concrete structures as the peak force levels experienced by the structure creates a limit point in which the Newton-Raphson iterations fail to converge (the tangent stiffness matrix is singular). Analysing the post-failure response of concrete structures with an implicit solver requires the problem to be reformulated into a displacement-controlled problem or to use an arc-length solution technique.

A more suitable solution technique for the analysis of the post-failure response of concrete structures is the explicit dynamic scheme. In explicit dynamic analyses, the solution obtained at each increment are

based on central differences without equilibrium iterations which makes the solution method extremely robust. However, the explicit scheme is formulated for dynamic problems and typically require very small time increments to satisfy the stability requirements of the central differences scheme (the CFL criterion). Nonetheless, explicit analyses may still be performed on quasi-static problems either through mass scaling or time scaling. The explicit scheme is suitable for highly non-linear problems where implicit methods are expected to not converge but comes with a relatively high computational cost.

When analysing existing structures with NLFEA, a large uncertainty is the state of the material in the structure. In concrete structures, different parts of the structure might be subject to different degrees of degradation which will affect the local stress distributions and should be included in the NLFEA model for the most accurate results. Mapping all the defects in a structure is a challenging task and, as such, defects are typically not included in NLFEA models unless they are very prominent. The concrete compressive strength in existing concrete structures is higher than the design values due to the age of the concrete. If the design compressive strength is used in NLFEA, as opposed to the actual compressive strength determined from cylinder compression tests, the NLFE analysis can lead to unreasonably high utilisation of the concrete in the structure.

The uncertainty of FE-models – both linear and non-linear – require careful engineering judgement from the analyst when interpreting the results. Even if the analyses show local overutilisation of the concrete structure, the actual structure might still be fine in an ultimate/accidental limit state due to effects and mechanisms not captured by the FE model. An engineer performing NLFEA should have a solid grasp on both structural mechanics, and computational mechanics to best interpret analyses results and to understand the limits of such analyses.

3 Advanced monitoring - Leveraging State-of-the-Art Technologies for Structural Integrity Evaluation

3.1 General

Traditional maintenance practices often rely on destructive testing methods, which can be time-consuming, costly, and disruptive to ongoing operations. As infrastructure networks continue to expand and age, the need for more efficient and non-destructive maintenance strategies has become increasingly crucial. This chapter explores the application of advanced monitoring technologies to address these challenges, and also how they can be used to serve input to NLFEA as a measure for performing enhanced structural integrity evaluation.

3.1.1 Drones: Unveiling Structures from Above

Unmanned aerial vehicles (UAVs), commonly known as drones, have emerged as powerful tools for structural monitoring. Their ability to access hard-to-reach areas and capture high-resolution imagery from above provides valuable insights into the condition of structures. Drones equipped with LiDAR (Light Detection and Ranging) sensors can generate detailed point clouds that accurately map the geometry of structures, revealing potential defects and deformations.

3.1.2 LiDAR: 3D Reconstruction and Defect Detection

LiDAR technology utilizes laser pulses to measure distances, creating a comprehensive 3D representation of a structure. This information can be used to identify and quantify structural anomalies, such as cracks, corrosion, and deformations. LiDAR data can also be integrated with other monitoring methods to provide a holistic understanding of a structure's health and performance.

3.1.3 Hyperspectral Imagery: Spectral Analysis for Defect Identification

Hyperspectral imaging captures images that contain information about the spectral characteristics of objects, enabling the analysis of their chemical composition and material properties. This data can be used to detect subtle changes in a structure's surface, indicating potential damage or deterioration.

3.1.4 Photogrammetry: 3D Modeling and Visualization

Photogrammetry utilizes multiple photographs taken from different angles to reconstruct a 3D model of a structure. This technique is particularly useful for structures with intricate geometries or complex surface features. Photogrammetry models can be used to create interactive visualizations, enabling engineers and inspectors to thoroughly assess the condition of a structure from any angle.

3.1.5 Handheld Ultrasound Scanners: Non-Destructive Evaluation

Handheld ultrasound scanners provide a non-invasive method for detecting and evaluating defects in concrete structures. These scanners emit high-frequency sound waves that penetrate the concrete and reflect back from internal defects, such as cracks, voids, and delaminations. The reflected waves can be analyzed to determine the location, size, and severity of defects.

3.1.6 Integrating Advanced Technologies for Comprehensive Monitoring

The integration of these advanced monitoring technologies offers a comprehensive approach to structural integrity evaluation. Drones provide aerial surveys, LiDAR generates 3D models, hyperspectral imagery identifies material variations, photogrammetry creates detailed models, and handheld ultrasound scanners detect internal defects. Together, these technologies can provide a holistic understanding of a structure's condition, enabling informed maintenance decisions and proactive interventions to extend the service life of infrastructure assets.

3.2 Robot and drones

Robots and drones are quite effective tool. Advanced monitoring technologies are revolutionizing the way we evaluate and maintain our aging infrastructure. By leveraging drones, LiDAR, hyperspectral imagery, photogrammetry, and handheld ultrasound scanners, we can gain unprecedented insights into the condition of structures, enabling predictive maintenance strategies that minimize downtime and prolong the service life of critical assets. As these technologies continue to advance, we can expect even more sophisticated and effective methods for structural integrity assessment, paving the way for a more resilient and sustainable infrastructure network.

The European Union's (EU) new drone regulation (EU) 2019/947, also known as Regulation 947, has introduced a landmark shift in the approach to regulating unmanned aircraft systems (UAS) or drones. This regulation, which came into force in December 2020, has revolutionized the landscape of drone operations, paving the way for their wider adoption in various sectors, including infrastructure maintenance.

At the heart of Regulation 947 lies the concept of proportional safety, which recognizes that the level of safety measures required should be proportionate to the level of risk associated with the drone operation. This approach has been instrumental in enabling the safe and efficient use of drones for structural integrity evaluation, particularly in sensitive environments like road bridges.

The proportional safety regime of Regulation 947 allows for the tailoring of safety requirements to the specific characteristics of each drone operation. This flexibility is particularly beneficial for large drones, which are often employed for high-altitude surveys and can provide detailed insights into the condition of structures.

However, the operation of large drones on road bridges can pose unique challenges. Height restrictions, restricted access, and the presence of sensitive infrastructure elements like power lines require careful planning and adherence to strict safety protocols.

In contrast, operating drones for structural monitoring on hydro-electric dams and offshore oil rigs is generally less restrictive. These environments typically offer open airspace and minimal interference from other infrastructure elements, allowing for more flexible drone operations.

The proportional safety approach of Regulation 947 recognizes these differences and allows for tailored safety regulations for each type of structure. For road bridges, stricter operational restrictions, such as lower altitude limits and designated flight paths, may be required to ensure public safety. For hydro-electric dams and offshore oil rigs, more permissive regulations may be applicable, allowing for more comprehensive drone surveys.

The proportional safety regime of Regulation 947 has not only facilitated the safe use of drones for structural integrity evaluation but has also encouraged the development of innovative drone-based inspection technologies. These advanced technologies, such as hyperspectral imaging and LiDAR, are enabling more detailed and precise assessment of structural conditions, leading to more efficient and cost-effective maintenance strategies.

As the use of drones for infrastructure maintenance continues to grow, the proportional safety approach of Regulation 947 will play a crucial role in ensuring the continued safe and responsible deployment of these technologies. By tailoring safety requirements to the specific risks associated with each operation, the regulation empowers drone operators to utilize these tools effectively while protecting public safety and environmental integrity.

The EASA drone regulation, with its emphasis on proportional safety, has opened up new possibilities for utilizing drones in infrastructure maintenance. This innovative approach is enabling the development of more efficient and cost-effective maintenance strategies, extending the lifespan of critical infrastructure assets, and ultimately, contributing to a more sustainable and resilient infrastructure network.

3.3 Advanced data handling and processing

The behaviour of a structure is the response resulting from the state of the structure and the load on the structure. The purpose of doing NLFEA is to model and predict the effect of the structure's condition on the response, and by incorporating data from the service life model, simulating the effect of further deterioration and damage mitigating measures on the response.

Data from service life survey will be collected and stored in a database. Data from pH- and humidity sensors, and corrosion gauges will supplement inspection data. The dataset will be input to the service life model, predicting – extrapolating – the development of the state of the structure with time.

Structural monitoring systems can continuously gather information regarding the structure through data acquisition from installed instruments and sensors. Data from sensors installed on and in the structure are collected and stored in the database. Such data could be from accelerometer, strain gauge, tilt meter, displacement gauge, and instrument recording wind speed and direction. The data must be processed to remove noise and to identify sensors that provide relevant information, describing the behaviour of the structure.

Accuracy and precision of the measurement data are important properties of a structural monitoring system. This is of importance with respect to data post-processing, data analysis and predictions to be performed. High data quality reduces uncertainty.

Data sampling, streaming and integration are parameters influencing how data can be processed. Continuous data processing and analysis are beneficial with respect to early detection and warning. Postponed data processing (months or years after the actual measurements) is beneficial with respect to mode trend analysis, model updating, risk analysis and calibration tasks. Data acquisition should be planned and conducted in a way that secures data consistency over time, to make trend analysis possible. The following topics and questions should be considered to provide relevant data for calibration of NLFEA and for trend analysis:

- What data are needed i.e., what sensors (Cosmin Popescu, 2023) are to be installed?
- Where should the sensors be installed i.e., location on and in the structure?
- How is data acquisition to be done?
- Where will the data be stored?
- What structure will the stored data have?
- What postprocessing of the data will be needed?

3.4 Detection of cracks and crack patterns

3.4.1 Photogrammetry

Concrete structures, ubiquitous in modern construction, are subject to various degradation factors, including cracking, which can significantly compromise their integrity and lifespan. Traditional non-destructive testing (NDT) methods for crack detection and mapping can be expensive, time-consuming, and may require access to restricted areas, limiting their widespread adoption.

In recent years, photogrammetry has emerged as a cost-effective, non-contact, and versatile tool for concrete crack detection and mapping. This technique utilizes multiple photographs taken from different angles to reconstruct a 3D model of a structure. By analyzing the distortions and changes in the surface texture of the model, cracks and their patterns can be identified and quantified.

Benefits of Photogrammetry for Crack Detection and Mapping

Photogrammetry offers several advantages over traditional NDT methods:

1. **Cost-effectiveness:** Photogrammetry requires no specialized equipment or software, making it a more affordable solution compared to laser scanning or radar technology.
2. **Non-contact:** Photogrammetry does not require physical contact with the structure, minimizing disruption to ongoing operations and reducing the risk of damage.
3. **Versatility:** Photogrammetry can be used to survey a wide range of concrete structures, including bridges, buildings, and pavements, regardless of their size or complexity.
4. **Rapid data acquisition:** Photogrammetry can capture data quickly and efficiently, allowing for regular inspections and monitoring of structural integrity over time.

3.4.2 Case Studies Demonstrating Photogrammetry's Effectiveness

Several studies have demonstrated the effectiveness of photogrammetry for crack detection and mapping in concrete structures. One study investigated the use of photogrammetry to monitor the cracking patterns in a bridge deck over a period of two years. The results showed that photogrammetry was able to accurately detect and quantify the growth of cracks, providing valuable insights into the bridge's condition and enabling proactive maintenance decisions.

Another study examined the application of photogrammetry to detect cracks in concrete pavements. The study found that photogrammetry could reliably identify cracks, even when they were small or shallow, and could differentiate between active and inactive cracks. This information was used to prioritize maintenance efforts and ensure the structural integrity of the pavements.

These case studies highlight the potential of photogrammetry as a reliable and cost-effective tool for crack detection and mapping in concrete structures. By utilizing this technology, infrastructure managers can gain valuable insights into the condition of their assets, enabling timely maintenance and extending the lifespan of critical infrastructure elements.

Photogrammetry has emerged as a promising tool for crack detection and mapping in concrete structures. Its affordability, non-contact nature, versatility, and rapid data acquisition capabilities make it a compelling alternative to traditional NDT methods. As photogrammetry technology continues to develop, its application in infrastructure inspection and maintenance is expected to expand further, contributing to a more efficient, cost-effective, and sustainable approach to managing our aging infrastructure assets.

4 Damage mechanisms

4.1 Exposure, deterioration, and durability

4.1.1 Exposure conditions

Concrete can withstand considerable chloride ingress or carbonation for several decades. Concrete in exposure class XC, XD, and XS has according to the standard (including recommendation) limitations to binder combination and the concrete composition, cover, as well as crack width (NS-EN206) (NS-EN1992). Any exceeding of these limitation can decrease the service life of the structure.

4.1.2 Permeability

Permeability is the ability of fluids and gases to flow through porous media like concrete under the influence of a constant pressure difference over the specimen. Darcy's law, se Eq. 1, is a simple proportional relationship between the instantaneous discharge rate through a porous medium (also called flux), the viscosity of the fluid and the pressure drop over a given media thickness.

$$Q = \frac{-\kappa \cdot A}{\mu} \cdot \frac{(P_b - P_a)}{L} \quad (1)$$

where

Q = total discharge [m³/s]

κ = permeability coefficient [m²]

(P_b – P_a) = constant pressure drop [Pa = N/m² = kg/m·s²]

μ = the dynamic viscosity of the fluid [kg/m·s]

L = length the pressure drop is taking place over (e.g. wall thickness) [m]

A = area of penetrated medium perpendicular to the direction of Q [m²]

Darcy's law is a simple mathematical statement which neatly summarizes several familiar properties, including:

- if there is no pressure gradient over a distance, no flow occurs (this is hydrostatic conditions),
- if there is a pressure gradient, flow will occur from high pressure towards low pressure (opposite the direction of increasing gradient - hence the negative sign in Darcy's law),
- the greater the pressure gradient (through the same formation material), the greater the discharge rate, and
- the discharge rate of fluid will often be different — through different formation materials (or even through the same material, in a different direction) — even if the same pressure gradient exists in both cases.

For composite materials such as concrete, modification of Darcy's law is necessary for calculation of permeability.

4.1.3 Diffusion

Diffusion (result of concentration gradients) through (steady state flow) porous media, e.g. concrete, can be modelled by a linear diffusion equation, Fick's 1st law, in the following form for one dimension;

$$C(x, t) = C_s - (C_s - C_i) \cdot \text{erf} \left(\frac{x}{2\sqrt{D \cdot t}} \right) \quad (2)$$

where

$C(x,t)$ = gas or liquid concentration in the concrete

C_s = gas or liquid concentration in the environment

erf = the error function

This is the most used equation to determine chloride permeability, both in water saturated concrete, and also in partly saturated concrete. Since the latter case is also affected by capillary absorption, it is called apparent diffusion coefficient (D).

The diffusion coefficient D , depends among other things on:

- Porosity
- Amount of cracks, crack widths and crack depths - w/c ratio
- Type of cement
- Degree of hydration
- Content of pozzolanas
- Exposure time, see (3)
- Temperature

The diffusion coefficient at different exposure time is often found to be well predicted by

$$D_{t_i} = D_{t_0} \cdot \left(\frac{t_0}{t_i} \right)^\alpha \quad (3)$$

where

D_{t_i} = the diffusion coefficient at time t_i

D_{t_0} = the diffusion coefficient at time t_0

α = aging parameter between 0 and 1, dependent on concrete and environment

4.1.4 Chloride diffusion coefficient in cracked concrete

When cracks occur in concrete structures, permeation of water and penetration of harmful ions (e.g., chloride ion) through the cracks may accelerate corrosion and deterioration of steel reinforcements, which can affect the serviceability of the structures (Jang, 2011).

$$D_{cr} = \frac{D_{eq} A_{tot} - D_{uncr} A_{uncr}}{A_{cr}} \quad (4)$$

Where:

D_{eq} is the diffusion coefficient determined for the cracked concrete (m^2/s)

D_{uncr} is the diffusion coefficient determined for uncracked concrete (m^2/s)

A_{cr} is the crack area (m^2)

A_{uncr} is the uncracked area (m^2)

A_{tot} is the total area (m^2)

Figure 4-1 below shows the increase of chloride diffusion coefficient in the cracked area (D_{cr}) in accordance with the increase of average crack width in the cracked specimens. The chloride diffusion coefficient in the cracked area is calculated using Eq. (4). The equation above is tested in combination with ultrasound in order to evaluate the water permeability and chloride ion penetrability of cracked concrete (Jang, 2011)

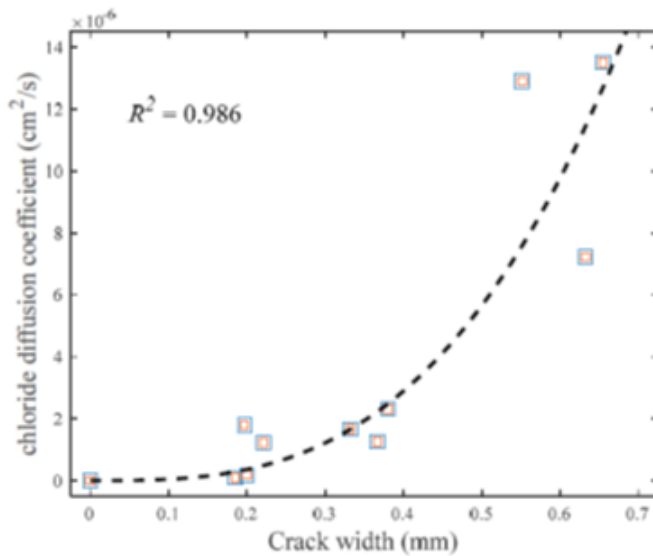


Figure 4-1: Crack width versus Chloride diffusion coefficient (Jang, 2011).

4.1.5 Mechanical Property development

The concrete gradually develops strength and stiffness during the hardening phase. The material properties development is depending on time and temperature. It can also be assumed that strength development is depending on the same parameters that controls the permeability in the concrete.

The *compressive strength* of concrete is a fundamental and much studied concrete property. Compressive strength is however relatively easy to determine, and is therefore often used in correlation with other properties such as tensile strength and E-modulus. At an engineering level (macroscale level), there are at least five different concepts which can be used to describe the development of compressive strength during the hydration process: the porosity concept, the gel-space ratio concept, the degree of hydration concept, the maturity principle and chemistry-oriented strength laws (Brugel, 2001).

Tensile strength can be determined directly by uniaxial tensile strength tests, or indirectly by splitting tensile strength tests or bending tests. The indirect tensile splitting test is considered favourable from a laboratory perspective due to the difficulties experienced with direct tensile methods.

The E-modulus can be determined both by compressive tests and tensile tests. Usually, the tensile and compressive E-modulus are assumed to be the similar or slightly higher tensile E-modulus compared to compressive E-modulus (Yoshitake, 2013).

The mechanical properties development has also been described by the maturity-based heat development model proposed by (Freiesleben Hansen, 1977).

The modified CEB-FIB MC 1990 can describe the development of the compressive strength, tensile strength, and modulus of elasticity.

Compressive strength:

$$f_c = f_{c28} \cdot \exp \left\{ s \left(1 - \sqrt{\frac{28}{t_{eq} - t_0}} \right) \right\} \quad (5)$$

Tensile strength (Kanstad, 2002):

$$f_t = f_{t28} \left\{ \exp \left[s \left(1 - \sqrt{\frac{28}{t_{eq} - t_0}} \right) \right] \right\}^{n_t} \quad (6)$$

Modulus of elasticity:

$$E_c = E_{c28} \left\{ \exp \left[s \left(1 - \sqrt{\frac{28}{t_{eq} - t_0}} \right) \right] \right\}^{n_E} \quad (7)$$

Where:

t_{eq} = equivalent time

t_0 = concrete age when the concrete start to set

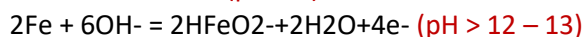
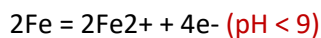
s = curve fitting parameter

n_t is curve fitting parameter for tensile strength and modulus of elasticity.

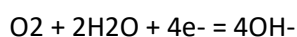
4.2 Reinforcement corrosion

Reinforcement corrosion occur when the passive film on the reinforcement is disrupted. The passive film on the reinforcement in the concrete can be unstable if the pH of the concrete is reduced to around 9 or in presence of chloride ions. At the anode the steel dissolves and corrosion products are formed. The type of corrosion products varies from voluminous solid products causing cracking and spalling to products with low volume and not necessarily causing visible damage.

At anode



At cathode



Carbonation will reduce the pH in the pore solution where calcium containing hydration product are transformed to calcium carbonate. When the carbonation front reaches the reinforcement, the pH-level in the pore solution will decrease and can initiate reinforcement corrosion.

Chloride initiated reinforcement corrosion occur when the threshold value for critical chloride content is exceeded and disrupt the oxide layer on the reinforcement.

The corrosion rate of the reinforcement depends on the oxygen admission to cathode, electric resistance in the concrete, and the anode/cathode ration.

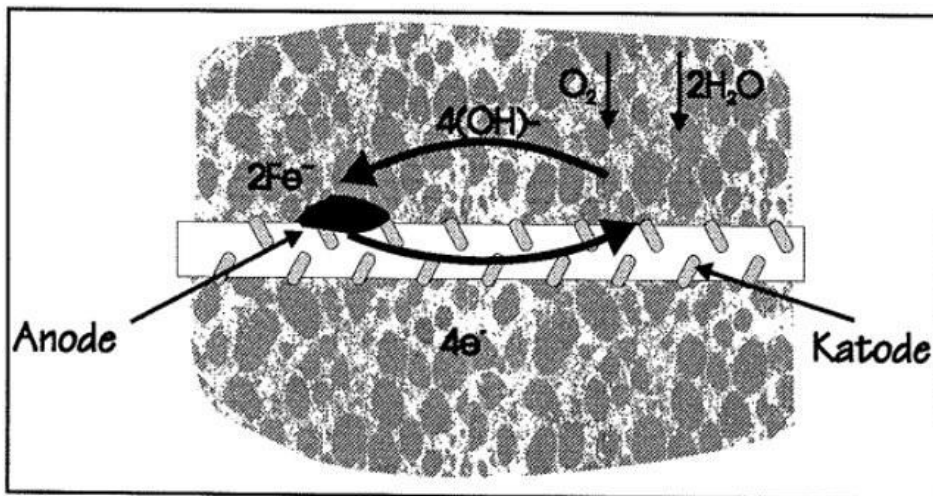


Figure 4-2: Corrosion process

4.3 Prestressing damages

This subsection will be included in the next revision of the document.

4.4 Alkali Silika Reaction

4.4.1 Reaction process

Alkali-silica reaction (ASR) is a deterioration mechanism in concrete caused by a physio-chemical reaction. Alkalis (Na^+ , K^+) and calcium hydroxide ($\text{Ca}(\text{OH})_2$) give a high pH in the concrete pore water, which increases the solubility of SiO_2 in certain aggregates so that it might partially dissolve. The reaction product is a swelling alkali-silica gel (ASR-gel) composed of silicon, sodium, potassium, calcium, oxygen, and hydrogen (Sims & Pool). A high internal humidity ($\text{RH} > 80\%$) is required for the reaction to take place, and normally higher moisture state increases the damage (Lindgård, 2013). The reaction and swelling mechanisms are very complicated and still uncertain. However, recently, Leemann et al. (Leemann, G'ora, Lothenbach, & Heuberger, 2024) proposed a detailed mechanism leading to the internal micro-cracking. The ASR-gel will induce internal pressure and micro-cracking in the aggregates and at a later stage in the cement paste, accompanied with an expansion of the concrete. The micro-cracks will also lead to a reduction of the mechanical properties of the concrete, especially the stiffness (E-modulus) and tensile strength.

Figure 4-3 shows the three main components that need to be present for the concrete to expand (alkali-reactive aggregates, alkalis, and water). If one of the components is below a certain critical limit, the reaction will not start (or it might stop, e.g. if the moisture state decreased sufficiently). ASR is, therefore, primarily a problem for structures exposed to high moisture, for example power plants, tunnel linings, retaining walls and massive outdoor structures, such as concrete dams and bridges. The extent and rate of the expansion vary between different areas and countries dependent on aggregate type, exposure conditions (moisture and temperature) and the alkali content of the cement paste. Local variations in the material composition and micro-climate (moisture conditions) will also greatly impact the extent of cracking and expansion. The expansion can be unevenly distributed both over the same structural member, between different members or over the cross-section.

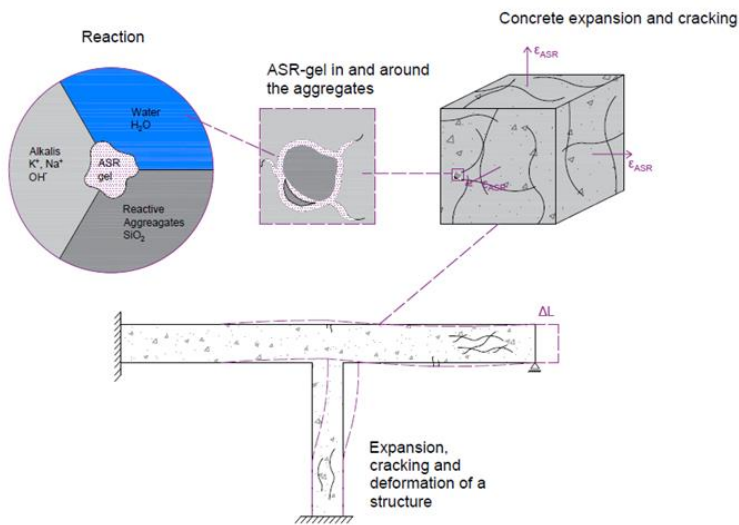


Figure 4-3: Damage mechanism of ASR, from the reaction to the expansion, cracking and deformation of a concrete structure

4.4.2 Damage mechanisms

In an outdoor environment, the outer layer of the concrete will alternately dry out and moisten. When the concrete in this layer dries out, it gets a certain shrinkage. Alkali-ions will also leach out of the surface layer (the depth influenced depends on several factors). Both these mechanisms make the expansion condition more favourable further into the concrete section. Both the effect of occasional shrinkage and a greater expansion further into the cross-section will give tensile stresses in the outer layer. The outer layer will crack when the tensile stresses exceed the tensile strength. On structures with large surfaces and limited restraint, the cracking typically forms in a characteristic map cracking pattern, as shown in Figure 4-4.

After cracking, the moisture situation in this area will change, as the cracks will hold on to more water before it dries. This effect will both give more favourable conditions for further expansion and might also "open up" for other deterioration mechanisms such as frost and reinforcement corrosion.



Figure 4-4: Characteristic map cracking on a surface due to ASR

In a reinforced concrete structure, only the concrete expands, but the bond between the reinforcement and the concrete will force the reinforcement to follow the concrete. This effect gives initial or additional

tensile stresses in the reinforcement and corresponding compressive stresses in the concrete in the reinforcement direction. Similar stress states will also occur if one part of a section expands more than other parts. If a structure is statically determinate, this effect can be handled locally. However, if the structure is statically indeterminate, e.g. restrained against the ASR expansion, these stresses will also result in additional loads and load resultants in the form of restraining moments and axial forces.

In NPRA Report 855, “*Assessment of bridges with alkali-silica-reactions – ASR*” (Johansen, 2022) and in (Stemland, Johansen, & Kanstad, Load Effects of ASR-induced Expansion in Reinforced Concrete and Their Consequences for Structural Assessment, 2023), the main structural consequences of the ASR expansion are described as:

- Direct consequences:
 - Initial stresses: Only the concrete expands. Due to the bond, the reinforcement is, however, forced to follow the concrete. This gives tensile stresses in the reinforcement and, due to equilibrium, compressive stresses in the concrete.
 - Restraint forces in statically indeterminate systems: The local rotations of each section and the overall elongation are partly prevented in such structures, leading to restraint moments and axial forces.
 - Change in the mechanical properties of the concrete: ASR is reducing the tensile and compressive strength and the E-modulus of the concrete, which again may result in reduced moment capacity, anchorage slip of the reinforcement and potential horizontal delamination of a bridge slab.
- Indirect consequences: The structural system and the boundary condition may change. This can be due to, for example, the closing of joints, which then initiates compressive forces in a dam or bridge structure and supports that are pushed out of their positions.

ASR may, therefore, lead to both increased loads and reduced capacity.

4.4.2.1 *Effect on material properties*

The internal cracking/micro-cracking due to ASR will lead to a degradation of the material properties of the concrete. The most affected properties are the tensile strength, the E-modulus and the compressive strength. The internal cracking will also lead to a more ductile behaviour, as shown on the stress-strain curves in (Kongshaug S. S., et al., 2020). Early in the 1990s, the *Institution of Structural Engineers* (ISE) (Institution of Structural Engineers, 1992) suggested a correlation between the expansion ($\% = \text{mm/m}$) and the compressive strength, tensile strength (splitting tensile strength) and the E-modulus, as shown in Table 4-1.

Table 4-1: Suggested relationship between the expansion in ‰ (mm/m) and different mechanical properties for concrete from Institute of Structural Engineers (Institution of Structural Engineers, 1992). The values are lower bounds relative to 28-day values for undamaged concrete

Property	Expansion [‰]				
	0.5	1.0	2.5	5.0	10.0
Compressive cube strength, $f_{c,cube}$	100	85	80	75	70
Compressive cylinder strength, $f_{c,cyl}$	95	80	60	60	-
Splitting tensile strength, $f_{ct,sp}$	85	75	55	40	-
E-modulus, E_c	100	70	50	35	30

From this table, except for the tensile strength, the properties only have limited reductions for an expansion of about 0.5 ‰. The reductions gradually increase from this level but are only significant at an expansion of about 2.5 ‰. The table is, however, relatively rough.

A relatively high E-modulus reduction is documented by several studies (Institution of Structural Engineers, 1992; Chrisp, Waldron, & Wood, 1993; Jones & Clark, 1998; Ahmed, Burley, Rigden, & Abu-Tair, 2003; Smaoui, Berube, Fournier, Bissonnette, & Durant, 2004; Esposito, Anac, Hendriks, & Copuroglu, 2016; Kongshaug S. S., et al., 2020; Stemland, Rodum, & Kanstad, 2022; Noël, Sanchez, & Tawil, 2017) (Sanchez, Fournier, Jolin, Mitchell, & Bastien, 2017), even by modest expansion levels, and is identified through the literature review by Esposito et al. (Esposito, Anac, Hendriks, & Copuroglu, 2016), as the best indicator of ASR damage. The size of the reduction will, however, vary depending on the material composition and type of aggregate used, as shown in (Ahmed, Burley, Rigden, & Abu-Tair, 2003; Giaccio G., Zerbino, Ponce, & Batic, 2008; Sanchez, Fournier, Jolin, Mitchell, & Bastien, 2017). This can also be illustrated in Figure 4-5, where the E-modulus reduction for specimens with increasing expansion levels ($\% = \text{‰}/10$) from the investigation by Kongshaug et al. (Kongshaug S. S., et al., 2020) using Norwegian aggregates, is shown with the upper and lower bounds from the investigation by Sanchez et al. (Sanchez, Fournier, Jolin, Mitchell, & Bastien, 2017), who tested a variety of aggregates and concrete mixes (concrete strengths). The E-modulus is in both investigations obtained using the Stiffness Damage Test (SDT), which is a mechanical stress-strain test consisting of five load cycles on a specimen up to 40 % of the 28-day strength, as described by Sanchez et al. (Sanchez, Fournier, Jolin, & Bastien, 2014).

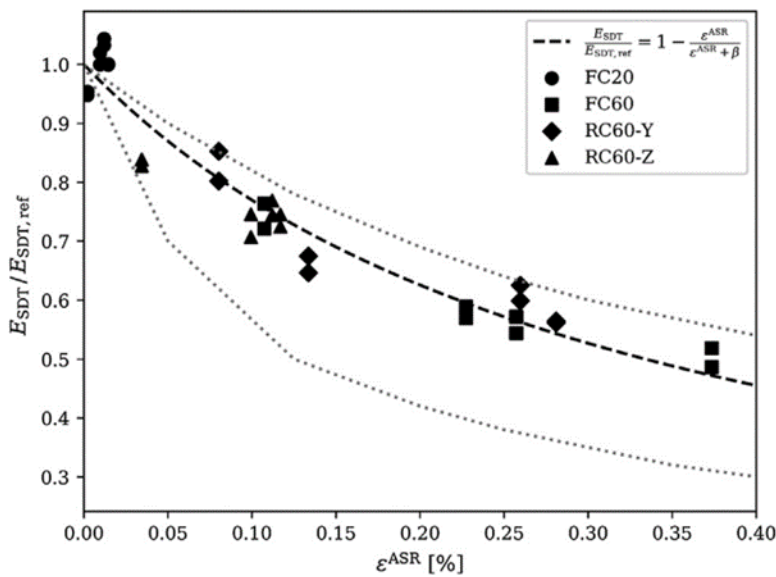


Figure 4-5: E-modulus reduction from Kongshaug et al. (Kongshaug S. S., et al., 2020) compared to upper and lower bounds from Sanchez et al. (Sanchez, Fournier, Jolin, Mitchell, & Bastien, 2017). The E-modulus are in both studies obtained using the Stiffness Damage Test (SDT) (From (Kongshaug S. S., et al., 2020))

The compressive strength has also been investigated by several studies (Institution of Structural Engineers, 1992; Giaccio G. , Zerbino, Ponce, & Batic, 2008; Esposito, Anac, Hendriks, & Copuroglu, 2016; Barbosa, Hansen, Hansen, Hoang, & Grelk, 2018; Kongshaug S. S., et al., 2020). Generally, the loss of compressive strength is much lower than the reduction in E-modulus and tensile strength, especially for moderate expansion levels. It is, therefore, not considered a good indicator of ASR damage. A challenge with this parameter is the simultaneous strength increase, which might compensate for the reduction due to ASR. Barbosa et al. (Barbosa, Hansen, Hansen, Hoang, & Grelk, 2018) did, however, find significant reductions for cores drilled perpendicular to quite extensive cracks on existing bridges in Denmark. A reduced compressive strength will affect the moment capacity in areas where the compression zone is highly utilized.

Due to the micro-cracking, the tensile strength could be significantly reduced at low expansion levels (Jones & Clark, 1998). This parameter is, however, quite dependent on the test method. Previous investigations on ASR-affected concrete have shown significant differences in tensile strength reduction depending on the test method (Institution of Structural Engineers, 1992; Jones & Clark, 1998; den Uijil & Kaptijn, 2002; Esposito, Anac, Hendriks, & Copuroglu, 2016; Noël, Sanchez, & Tawil, 2017; Barbosa, Hansen, Hansen, Hoang, & Grelk, 2018; Ahmed, Burley, Rigden, & Abu-Tair, 2003). Uijil and Kaptijn (den Uijil & Kaptijn, 2002) tested cores from existing slab bridges and found a reduction of the tensile strength of about 10-20 % from the splitting test, while the reduction was up to 70 % for the uniaxial test. The splitting tensile test has also shown a more even reduction (Institution of Structural Engineers, 1992) compared to the uniaxial test and, in some cases, a slight initial increase (Ahmed, Burley, Rigden, & Abu-Tair, 2003; Esposito, Anac, Hendriks, & Copuroglu, 2016). The difference is probably because the splitting tensile strength test will distribute the tension stresses over a larger area, while the uniaxial strength test will, to a greater extent, be controlled by weak areas or cracks. The tensile strength is usually neglected in the ultimate limit state. The bond properties and anchorage lengths of the reinforcement may, however, be influenced. A reduced tensile strength will also reduce the shear capacity.

Several studies have investigated the shear capacity of ASR affected beams (Chana & Korobokis, 1991; Bach, Thorsen, & Nielsen, 1993; den Uijil & Kaptijn, 2002; Schmidt, Hansen, Barbosa, & Henriksen, 2014; Bilodeau, et al., 2016; Hansen & Hoang, 2019; Noël, Sanchez, & Tawil, 2017; Hansen, Barbosa, Cao, & Hansen, 2016; Schmidt, Hansen, Barbosa, & Henriksen, 2014; Aryan & Gentruck, 2021), both on laboratory-cast beams and members from existing structures. Both reduced (Chana & Korobokis, 1991; den Uijil & Kaptijn, 2002) and increased (Bilodeau, et al., 2016; Bach, Thorsen, & Nielsen, 1993; Hansen, Barbosa, Cao, & Hansen, 2016) capacities from ASR are found. The primarily contributor to the increased capacities is the compressive stress that initiates in the concrete from the reinforcement, denoted the “chemical prestressing” effect.

4.4.2.2 *Effect of compressive stresses*

Compressive stress on a specimen will influence the internal stress state and the orientation of the micro-cracks. This will reduce the expansion in the stressed direction. This has been reported in several studies (Kongshaug S. S., et al., 2020; Zahedi, Trottier, Sanchez, & Noël, 2022; Larive, 1997) (Institution of Structural Engineers, 1992; Jones & Clark, 1998; Kawamura & Iwahori, 2004; Multon & Toutlemonde, 2006; Berra, Faggiani, Mangialardi, & Paolini, 2010; Dunant & Scrivener, 2012; Kagimoto, Yasuda, & Kawamura, 2014; Gautam, Penesar, Sheikh, & Vecchio, 2017; Wald, Allford, Bayrak, & Hrynkyk, 2017; Allard, et al., 2018). The compressive stresses can either be from an external force on the structure or from the reinforcement. Generally, higher stresses lead to more significant expansion reductions. Larive (Larive, 1997) did, however, conclude that compressive stress does not inhibit the reaction but only the expansion. Berra et al. (Berra, Faggiani, Mangialardi, & Paolini, 2010) showed a zero strain at stresses as low as 2 MPa, while Allard et al. (Allard, et al., 2018) observed low expansions of about 0.3 ‰ even at a stress level of 20 MPa. Berra et al. (Berra, Faggiani, Mangialardi, & Paolini, 2010) also showed that the size of the reduction and at which stress level the expansion stopped varied with different aggregates and alkali levels. Leemann et al. (Leemann, G'ora, Lothenbach, & Heuberger, 2024) showed that the ASR-gel can have a swelling pressure from 6-13 MPa in investigations with a synthetic gel.

Some studies also claim that the restraint/stress in one or several directions also increases the expansion in the stress-free directions. Different studies do, however, show quite variable results, from a clear effect with increasing free expansions at increasing stress levels/reduced expansion in restrained directions (Gautam, Penesar, Sheikh, & Vecchio, 2017; Multon & Toutlemonde, 2006) to only a slight effect in other studies (Larive, 1997; Berra, Faggiani, Mangialardi, & Paolini, 2010; Kagimoto, Yasuda, & Kawamura, 2014). Some investigations also have no such effect (Jones & Clark, 1998; Kongshaug S. S., et al., 2020; Dunant & Scrivener, 2012). This effect is, therefore, also probably quite material dependent, as stated by Berra et al. (Berra, Faggiani, Mangialardi, & Paolini, 2010), who showed that the effect differs with the amounts of alkalis and type of aggregates used.

The directional dependency of the expansion in a structure due to reinforcement or external load will also make the material behaviour anisotropic. The ASR-induced cracking is usually oriented in the main compressive stress direction/reinforcement direction, leading to a greater reduction of the material properties in the direction perpendicular to the cracks (the direction with the highest expansion), as reported in (Jones & Clark, 1998; Barbosa, Hansen, Hansen, Hoang, & Grell, 2018; Kongshaug S. S., et al., 2020).

5 Numerical modelling

5.1 General

There exist many different numerical modelling approaches and implementations of models for reinforced concrete structures and no clear consensus on the best method. The complexity of the plain concrete due to its meso- and microstructure as a heterogenous material and its composite action with reinforcing steel as well as variety and huge number of structural applications for reinforced concrete has led to the development of multitude methods. The non-exhaustive overview of the most currently applied numerical models that can capture damage and non-linear effects in mechanical performance of concrete is made based on the systematic literature search over the past six years. The search is related to the research literature and is thus aiming to identify research front and current knowledge and not the state of practice within industry. Therefore, the practical applicability of the identified methods is considered, and only numerical modelling approaches available through commercial or open-source software are considered.

5.1.1 Systematic literature search

The literature review was performed in a systematic way and the search regime is described below together with original search results for replicability and potential future updates of the systematic review.

Keywords and databases:

Database: Science Direct

Dates of search: 27.09.2023, 04.10.2023

Keyword:

'reinforced' AND 'concrete' AND ('non-linear model' OR 'material model') AND ('damage' OR 'failure' OR 'crack') NOT 'fiber' NOT 'fire'

Exclusion and inclusion criteria:

The literature search is limited to English-language-written articles published in the last 10 years. As can be noticed in the keyword, the fibre-reinforced and fire-exposed concrete are excluded.

Search statistics:

Due to the large list of articles the search was refined to include the specified keyword in title and abstract (as well as in the whole paper). The search with keywords on titles and abstracts only yielded 381 results, out of which 370 were research articles, 2 were review articles, and 4 were book chapters within the last 10 years (2013-2023). Most articles are published in Engineering Structures (98), Construction and Building Materials (37) and Structures (24). The statistics for the last six years are summarized in the table 5.1.1. Further analysis of the collected literature sample is restricted to the research and review articles only. For each article, the abstract, methodology for numerical model and conclusions from numerical model were read and if no relevant information were found the article was rejected. The relevant articles were read in more detail to identify the numerical modelling approach and classify according to the categories shown in Table 5-1.

Table 5-1: Research literature results in the last six years (2018-2023).

Search statistics			Identified numerical modelling approach				
year	results	After rejection criteria	Concrete damaged plasticity	Smearred orthogonal crack model	Plastic-fracture model	Cohesive zone model	Other
2023	51	9 ¹	4	1	2		2
2022	58	19 ²	9	3	2		4
2021	44	14 ³	8	2		2	2
2020	39	8 ⁴	4	4		1	
2019	32	11 ⁵	5	3		2	1
2018	30	14 ⁶	6	3		3	2
sum	254	65	36	16	4	8	11

The examination of the titles of the research articles has left following articles relevant:

- (2023) (He & Fan, 2023), (Hasan, Qasem, Muhamad, & Mutafi, 2022), (El-Joukhadar, Dameh, & Pantazopoulou, 2023), (Alfaiate & Sluys, 2023), (Yang, Wang, Yang, & Wang, 2023), (Jingfeng, Ziming, Shen, Guoqiang, & Zhenghu, 2023), (Basha, Tayeh, Maglad, & Mansour, 2023), (Wang, Pan, Zhao, & Zeng, 2023), (Guner, 2023)
- (2022) (Wani, Khan, & Vemuri, 2022) (Zhu & Ren, 2022), (Qasem, Hasan, Muhamad, & Mutafi, 2022), (Wang, Song, & Nie, 2022), (Panahi & Genikomsou, 2022), (Paz, Marques, & Ruas, 2022), (Hafiz, Schumacher, & Raad, 2022), (Alanazi & Susmel, 2022), (Wang, Le, & Ren, 2022), (Osmolska J. , Kanstad, A.N., & G, 2022), (Hernández-Díaz, Pérez-Aracil, Casillas-Perez, Pereira, & Salcedo-Sanz, 2022), (Dobry, Wolfger, & Benko, 2022), (Peng, Qiu, & Jiang, 2022), (Hasan, Qasem, Muhamad, & Mutafi, 2022), (Li, Guo, Jin, Zhang, & Gong, 2022), (Rad, Ibrahim, & Lógó, 2022), (Abdel-Jaber & El-Nimri, 2022)
- (2021) (Zhong, Zhuang, Shiyang, & Zhou, 2021), (Shirzehhagh & Fakhimi, 2021), (Alami, Fekak, Garibaldi, & Elkhalfi, 2021), (Sun & Zhu, 2021), (Guo, Dong, Bastidas-Arteaga, & Gu, 2021), (Nascimbene & Bianco, 2021), (Tao, Ren, & Chen, 2021), (Slowik, Novák, Novák, & Strauss, 2021), (Peng & Qiu, 2021), (Zhang & Wang, 2021), (Zhao, Lehman, & Roeder, 2021), (Taresh, Yatim, & Azmi, 2021), (Al-kroom, Reimer, Alghrir, Thneibat, & Schmid, 2021), (Srivaranun, et al., 2021)
- (2020) (Faron & Rombach, 2020), (Lee, Abolmaali, Shin, & Lee, 2020), (Goh & Hrynyk, 2020), (Kueres & Hegger, 2020), (Abra & Ftima, 2020), (Wang, Hayashida, Zhang, Gong, & Ueda, 2020), (Gomes, et al., 2020), (Senturk, Pul, Ilki, & Hajirasouliha, 2020)
- (2019) (Borbon-Almada, 2019), (Kurumatani, Soma, & Terada, 2019), (Rombach & Faron, 2019), (Castaldo, Gino, & Mancini, 2019), (Nasiri & Liu, 2019), (Marzec, Tejchman, & Mróz, 2019), (Wang, Gong, Zhang, Wang, & Ueda, 2019), (Chang, Lee, Carr, & Dhakal, 2019), (Dey & Karthik, 2019), (Chen J.-Y. , Li, Han, Wang, & Mu, 2019), (Fei, Yang, & Sun, 2019)
- (2018) (Allam, Elbakry, & Arab, 2018), (Hanif, Ibrahim, Ghaedi, H., & Javanmardi, 2018), (Castaldo P. , Gino, Bertagnoli, & Mancini, 2018), (Xi, S.Yang, & Li, 2018), (Benakli, Bouafia, Oudjene, Boissière, & Khelil, 2018) (Yang, Li, & Li, 2018), (Bao, Feng, Ma, Zhu, & Rabczuk, 2018), (Cervera, Tesei, & Ventura, 2018), (Dias-da-Costa, Cervenka, & Graça-e-Costa, 2018), (Liu & Su, 2018), (Hájková, Šmilauer, Jendele, & Červenka, 2018), (Chen Z. , Li, Yang, Zhao, & Fu, 2018), (Terán & Haach, 2018), (Alhanaee, Yi, & Schiffer, 2018)

The examination of the review articles revealed that only one is relevant: '*Damage assessment of reinforced concrete structures using a model-based nonlinear approach – A comprehensive review*' by (Hanif, Ibrahim, Ghaedi, H., & Javanmardi, 2018). The article focuses on vibration modelling incorporating non-linear behaviour for the purpose of damage detection in structural health monitoring of concrete structures. The authors state the gap in the current damage assessment of infrastructure of not including the non-linear effects caused by the damage into model behaviour. This is the gap that Excon project is addressing. The authors, however, focus on the methods compatible with Structural Health Monitoring (HSM), namely vibration analysis (modal analysis, linear dynamic analysis) which need to be extended to include non-linearities. The authors propose including concrete damaged plasticity (CDP) model as the nonlinear material modelling approach to dynamic finite element analysis for damage level assessment in reinforced concrete structures.

The criteria for rejection of articles were: models dedicated to non-traditional cement mixes (waste incineration tailings), blast, explosion, extreme water forces, tornado-induced collapse and impact analysis,

models of specific connector types (e.g., shear key), other materials than concrete (e.g., masonry, ground, soil), research directly focused on seismic loads and earthquake engineering, environmental assessment models, expansion joints models, steel-concrete composites, signal processing models, load estimation models, partial safety factor format in non-linear analysis, bridge management system models, retrofitting of RC structures, carbon nanotubes modified concrete, bentonite, decision-making models, geosynthetic reinforcement, concrete hollow bricks, critical shear displacement theory model, soil structure interaction, pushover analysis, model order-reduction techniques, operational modal analysis and model updating techniques, analytical model.

5.1.2 Pioneering work identified via cross-referencing of recent literature:

'*Analysis of crack formation and crack growth in concrete by means of fracture mechanics and finite elements*' was published by (Hillerborg, Mod er, & Petersson, 1976) who introduced a method compatible with finite element method to model cracks via a cohesive zone. A cohesive zone model predefined crack location and uses traction-separation laws as softening behaviour definition simulating crack growth.

'*A description of micro-and macroscale damage of concrete structures*' was published in 1986 by (Mazars, 1986), where micro cracking is believed to be the underlying reason for damage development within the concrete and damage is decomposed into compressive and tensile components.

'*A plastic-damage model for concrete*' was published in 1989 by (Lubliner, Oliver, Oller, & E. O ate, 1989). The constitutive plasticity model is introduced with a new yield criterion dedicated to concrete and the damage model is combined to account for different behaviour in compression and tension. The model is the basis for concrete damaged plasticity model implementation in ABAQUS.

'*A constitutive theory for the inelastic behavior of concrete*' was published in 1985 by (Ortiz, 1985). The anisotropic (compression and tension) behaviour damage is addressed in one framework and generalization to rate dependency is possible.

'*A Damage mechanics constitutive theory for the inelastic behaviour of concrete*' was published in 1987 by (Resende, 1987). Damage mechanics for inelastic degradation and plasticity for hydrostatic compression are combined in a rate-independent model.

'*Strain- and stress-based continuum damage models—I. Formulation*' was published in 1987 by (Simo & Ju, 1987). An elastoplastic rate-independent damage model is proposed in the two non-equivalent formulations (stress- and strain-based).

'*On energy-based coupled elastoplastic damage theories: Constitutive modeling and computational aspects*' was published by (Ju, 1989). A strain-based formulation of damaged plasticity for computational efficiency is developed.

'*Plastic-damage model for cyclic loading of concrete structures*' was published in 1998 by Lee and Fenves. Damage based on fracture energy and elastic degradation for compression and tension and tensile yield surface are introduced as three failure modes and scalar degradation model of the crack opening and closing effect is included. It is implemented within ABAQUS.

'*The modified compression-field theory for reinforced concrete elements subjected to shear*' was published in 1986 by Vecchio and Collins (Vecchio & Collins, 1986). The theory is an analytical model (constitutive equations) for the reinforced concrete under in-plane shear and compression/tension stress. Stress and strains within reinforced concrete are averaged and concrete is considered cracked (new material).

'*Non-orthogonal cracks in a smeared finite element model*' was published in 1985 by de Borst and Nauta (Borst & Nauta, 1985) and is based on the decomposition of the total strain into crack and concrete increments. The theory of plasticity, creep, and thermal shrinkage are incorporated in the new smeared model (Mazars, 1986).

'*Non linear analysis of frictional materials*' was published in 1986 by de Borst as his doctoral thesis and contains the strain decomposition concept to connect plastic and fracture theories, which was later a basis for the elastoplastic fracture model implemented in commercial software ATENA.

Constitutive Relations for Concrete was published in 1975 by (Chen & Chen, 1975). The model considers three three-dimensional stress states and stress-hardening plasticity low, weaker tensile strength as well fracture for finite element analysis of reinforced and prestressed concrete structures. The model is a reference for the fracture-plastic model implementation in ATENA software.

'*Constitutive Model for the Triaxial Behaviour of Concrete*' was published in 1975 by (WILLAM & WARNKE, 1975) and is now commonly referred to as the William-Warnke yield criterion as well as implemented in the commercial software ANSYS for concrete damage model based on plasticity.

5.2 NLFEA of concrete structures

5.2.1 General

Non-linear finite element analysis requires iterative methods to solve incremental equations of static or dynamic and find equilibrium (e.g., implicit solver based on the Newton-Raphson method) or to employ a very small time increment to ensure correct solution (explicit solvers). The non-linearity can be divided into three main types:

- Material non-linearity (damage, plasticity, cracking, crushing)
- Geometrical non-linearity (large displacements and rotations, sudden change of stable state, second order effects, pre-stress, stress stiffening)
- Boundary condition non-linearity (contact)

The general division of the material models developed to predict the nonlinear behaviour of reinforced concrete (RC) can be made based on the deriving method:

- Experimentally derived RC material models
- RC material models based on plasticity and fracture mechanics theory
- The damage in RC is predominantly caused by concrete cracking. The cracking can be modelled assuming two general approaches, as suggested by (Rots & Blaauwendraad, 1989):
- Discrete crack - the localized strong geometrical discontinuity
- Smeared crack - the cracked continuum represents the real discontinuities

Numerous implementations of both discrete and especially smeared crack models are present in the literature and the further division of the smeared crack models can be made into two main groups:

- Scalar plastic damage
- Stiffness degradation damage

The first group of models are more complex and difficult to implement and require extensive calibration of material parameters, while the second group of models suffer from mesh sensitivity and requires proper length scale selection for the element size and careful handling of complex stress states.

Several different models identified within literature published within the last six years are summarized below with detailed descriptions of those more frequently mentioned and applied.

5.2.2 Material modelling of concrete

5.2.2.1 Damaged plasticity model

A constitutive model based on plasticity theory to include smeared cracking of RC as well as differentiate between tensile and compressive strength is based originally most commonly on the work of Lubliner (Lubliner, Oliver, Oller, & E. Oñate, 1989) and (Lee & Fenves, 1998), who proposed a smooth yield surface that considers anisotropy of the concrete in tension and compression and non-associated plastic flow rule (to account for the anisotropy within shear deformations and volume change in concrete).

Concrete damaged plasticity (CDP) model was utilized in the following works published recently: Isotropic plastic damage model implementation, namely continuous surface cap model was used by (He & Fan, 2023) to model plain, and RC beams with and without stirrups. Precast RC wall under lateral load was modelled by (Hasan, R., M., & Muhamad, 2023). Strain energy limit criterium for plastic behaviour onset in the reinforced haunched beams was optimized using laboratory calibrated damage plasticity model by (Rad, Ibrahim, & Lógó, 2022). A comparison of the evaluation methods for the RC wall panels capacity between standards (American, European, Australian, and British) as well as numerical analysis in ABAQUS by (Abdel-Jaber & El-Nimri, 2022) show influence of slenderness, compressive strength and reinforcing ratio and their non-linear interaction. The connection between RC wall panels is a focus of (Hasan, Qasem, Muhamad, & Mutafi, 2022) and concrete damaged plasticity is used for concrete with smeared bilinear law for steel. A probabilistic analysis of the nuclear containment structure based on the concrete damage plasticity model for RC concrete and Ramberg-Osgood constitutive relationship for prestressing tendons was performed in (Li, Guo, Jin, Zhang, & Gong, 2022).

Modelling of pit-corrosion induced damage in concrete with radial expansion of the rebar and concrete damage plasticity as well as rebar-concrete bond-slip contact behaviour in mesoscale is shown in (Alami, Fekak, Garibaldi, & Elkhalfi, 2021). Concrete damaged plasticity model was used to simulate the behaviour of mortar and interface transition zone within mesoscale model of the RC slab under four-point bending test by (Jin, Wang, Zhang, & Du, 2021), while aggregate was modelled as elastomer. However, in (Peng & Qiu, 2021), concrete damaged plasticity was used to model all three concrete phases of mortar, interface transition zone and aggregate, while elasticity was assumed for pores in concrete to simulate the damage induced by freeze and thaw cycles in the mesoscale based on multi-scaling technique and use the damaged constitutive model in the macro-mechanical simulation of RC column.

Four different concrete models based on plasticity and available in LS-DYNA commercial software were compared by (Zhao, Lehman, & Roeder, 2021) for the cycling load simulation of the RC column on the feet and concrete damaged plasticity model was shown to provide best agreement with experiments. Punching shear in the slab-column connection was investigated by (Taresh, Yatim, & Azmi, 2021) for the effect of strengthening on the increase in capacity and ductility by experiments and numerical simulations employing concrete damaged plasticity model as implemented in ABAQUS. RC slab with saw-tooth connector was tested and modelled by (Al-kroom, Reimer, Alghrir, Thneibat, & Schmid, 2021) using plastic damage model in ANSYS based on Menetrey-Willam yield criterion with both smeared and explicitly modelled rebars. RC beams externally post-tensioned with steel rods are simulated using CDP model and no bond-slip by (Lee, Abolmaali, Shin, & Lee, 2020). Corroded RC beams were modelled using CDP model with parameters obtained via machine learning models based on experiments from 107 beams from literature and influence of non-linear geometry was investigated in (Alabduljabbar, et al., 2020). Shear cracks propagation in RC beams without transverse reinforcement under bending load is modelled using concrete damaged plasticity and compared to discontinues crack model with XFEM showing a good

agreement with experiment are presented in (Rombach & Faron, 2019) and (Faron & Rombach, 2020), see Figure 5-1, while stressing the high computational cost and continuous research and development stage of the methods.

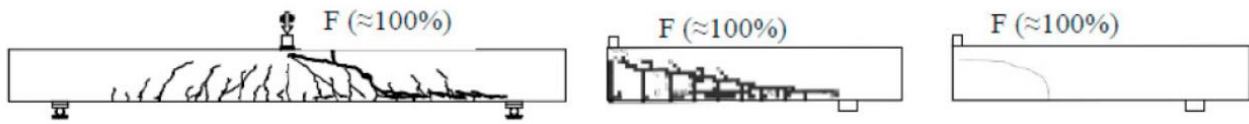


Figure 5-1: Comparison of crack patterns from experiment (left) and numerical simulations with smeared cracking using CDP model (centre) and discontinues cracking using XFEM (right). From (Rombach & Faron, 2019).

The reinforced concrete frame with infill is modelled in ABAQUS by Nasiri in (Nasiri & Liu, 2019) using CDP model and cohesive zone model for interaction with focus on out-of-plane behaviour under different geometrical parameters. The enhanced (non-local stiffening) elastic-plastic-damage model for RC was experimentally verified on different sizes of beams in a 4-point bending test by Marzec et al in (Marzec, Tejchman, & Mróz, 2019). New finite elements for RC analysis were developed to use together with concrete damaged plasticity model (Chang, Lee, Carr, & Dhakal, 2019). Several different material parameters for CDP model were used for concrete under different confinement conditions within the composite concrete-encased concrete-filled steel tubular structure in (Chen J.-Y., Li, Han, Wang, & Mu, 2019). A joint within the reinforced concrete frame was modelled using CDP model in ABAQUS by Allam (Allam, Elbakry, & Arab, 2018). CDP model was used as an example within the review article on damage assessment in RC (Hanif, Ibrahim, Ghaedi, H., & Javanmardi, 2018) to deal with uncertainties of linear vibrations analysis (response spectrum). A simplified model to avoid explicit incorporation of rebars within finite element analysis based on the explicit definition of constitutive laws for combined concrete and reinforcement interaction is compared to the CDP model by (Cervera, Tesei, & Ventura, 2018), (Dias-da-Costa, Cervenka, & Graça-e-Costa, 2018), (Benakli, Bouafia, Oudjene, Boissière, & Khelil, 2018). CDP model of the RC sewer box shows an estimation error below 15% compared to the experiment (Bao, Feng, Ma, Zhu, & Rabczuk, 2018). Large silo structure cracking due to temperature fluctuations is modelled with concrete damaged plasticity model by (Chen Z., Li, Yang, Zhao, & Fu, 2018).

Nuclear reactor containment capacity was estimated with concrete damaged plasticity model (ABAQUS) by (Alhanaee, Yi, & Schiffer, 2018). A bi-scalar plasticity damage model with Lubliner yield surface was implemented within peridynamic theory of handling discontinuities by (Zhu & Ren, 2022). Beam-column joint from precast RC was modelled using CDP with continuum elements and plasticity for reinforcements with truss elements and bond-slip model by (Qasem, Hasan, Muhamad, & Mutafi, 2022). Comparison of punching shear modelling with CDP and plastic-fracture model Cementitious2 is made by (Panahi & Genikomsou, 2022). A Willam-Warnke yield surface for the plastic damage model within ANSYS is applied to analysis of the massive concrete cracking due to thermal effects. (Basha, Tayeh, Maglad, & Mansour, 2023) has investigated the shear capacity of RC pile caps by varying reinforcement position in the numerical model based on CDP. RC columns with high-strength reinforcing steel were modelled with CDP showing the buckling failure mode by (Jingfeng, Ziming, Shen, Guoqiang, & Zhenghu, 2023). Early age cracking of massive concrete with embedded piping is modelled together with creep effects included via subroutine into damaged plasticity model in Ansys by (Wang, Song, & Nie, 2022).

The damaged plasticity model for concrete assumes two main failure mechanisms occurring in reinforced concrete depending on the stress state:

- Crushing under compression
- Cracking under tension

Both responses are linear elastic until the strength criterion for compressive and tensile stresses is reached. The crushing of concrete under compression is modelled using plasticity with stress hardening and subsequent strain softening that captures phenomenologically the real physical concrete behaviour. The cracking of concrete under tensile stress is realised via immediate softening. Both nonlinear stages result in unrecoverable damage D (D_t, D_c defined for tensile and compressive damage respectively) that is used as a scalar to degrade the initial elastic properties:

$$E_d = E(1 - D), \quad D \in \langle 0, 1 \rangle, \quad \boldsymbol{\sigma} = (1 - D)\mathbf{E} : (\boldsymbol{\varepsilon} - \boldsymbol{\varepsilon}_p) = (1 - D_t)\boldsymbol{\sigma}_t + (1 - D_c)\boldsymbol{\sigma}_c \quad (8)$$

where E_d is the new stiffness, and $\boldsymbol{\sigma}, \boldsymbol{\varepsilon}, \boldsymbol{\varepsilon}_p$ are the stress, strain, and plastic strain tensors respectively, see Figure 5-2. Damage accumulation is important for cycling loading when unloading and reloading are present and new degraded stiffness is used. The damage is defined as a percentage based on the amount of plastic strain or cracked strain. Those data are obtained experimentally in the cycling tension and compression tests. Reinforcement within the concrete damaged plasticity model is added by modifying material properties. Thus, the interaction between the concrete and steel, the bond slip, must be added separately within the post-tension stiffening model. This behaviour can be defined via stress-strain data or via stress-displacement (fracture energy) data. Those correspond to uniformly or sparsely reinforced concrete respectively and are subject to mesh sensitivity issues if used outside typical conditions. Stress-strain definition of tension stiffening works best for distributed reinforcement while the stress-displacement definition requires proper element length and ratio in the mesh generation.

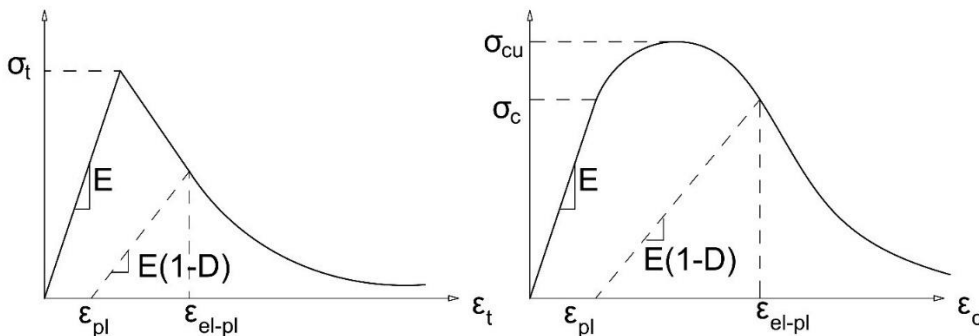


Figure 5-2: Uniaxial stress-strain curves in tension (left) and compression (right) used in the CDP model.

Yield surface commonly used within concrete damaged plasticity model is depicted in Figure 5-3 bottom right corner. CDP model requires definition of elastic, plastic, and damage (for non-monotonous loads) properties. Stress-strain data from uniaxial compression and tension tests (cylinder test) or the corresponding models from codes (e.g., EC2, Model Code 2010) for a given concrete class strength can be used. Young's modulus and Poisson ratio need to be specified for elastic part. Compression stress-strain tabular data for inelastic response under compression is required and the softening (stress-cracking) relationship can be chosen between several laws, see Figure 5-3.

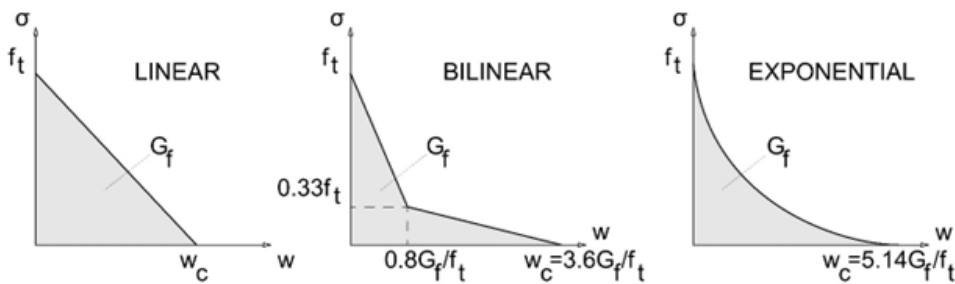


Figure 5-3: Tension softening stress-crack opening curves: linear (left), bilinear by Hillerborg (centre), and exponential by Cornelissen (right).

Additionally, the plasticity theory data about the potential flow, e.g., shear dilation angle (change in volume associated with shear deformation due to reconfigurations in the microstructure, observed in granular materials (Vermeer & Borst, 1984)), biaxiality ratio under compression, plastic flow eccentricity, ratio of second stress invariants in compression and tension, and viscosity need defining.

When damage accumulation is defined, the damage must increase monotonically with increasing plastic strains (unrecoverable strains) and cannot lead to the negative plastic strains ($\varepsilon_{pl} \geq 0$).

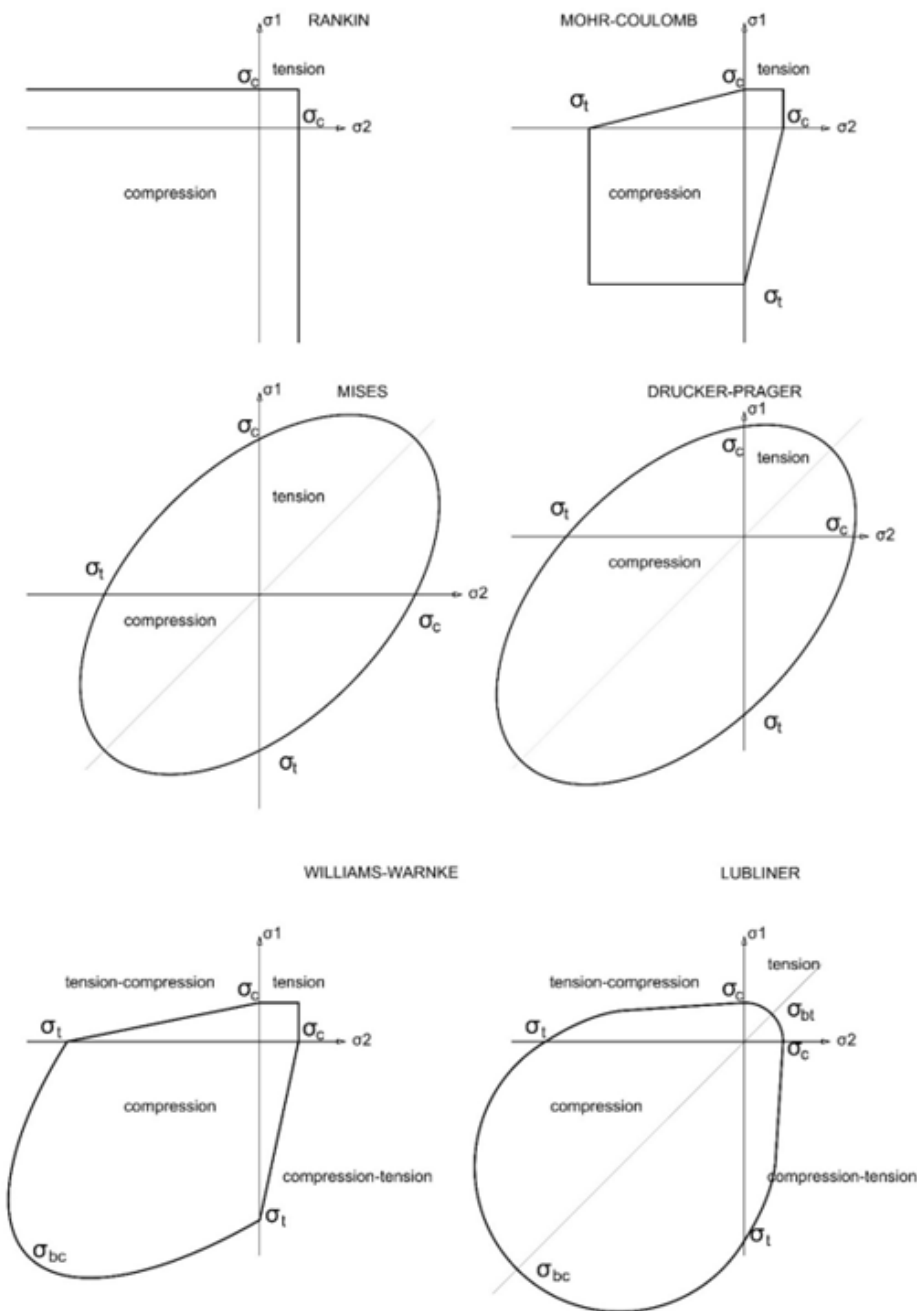


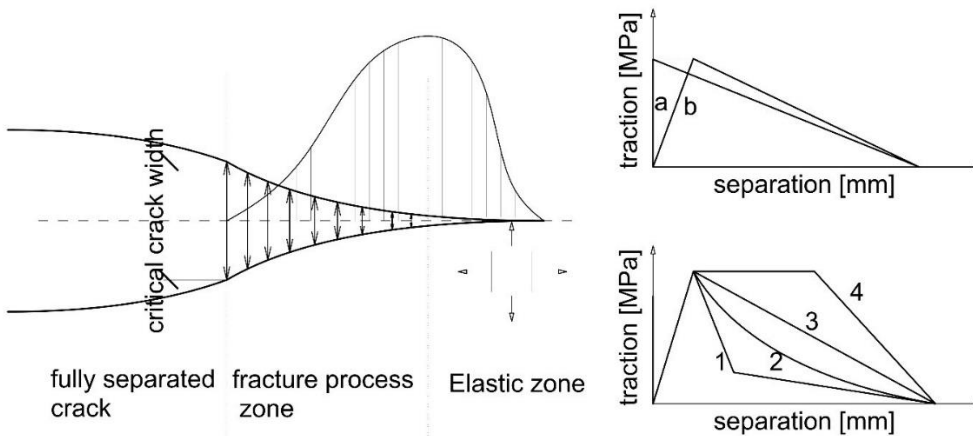
Figure 5-4: Strength limits/ yield surfaces used for reinforced concrete modelling shown in principal plane stress space.

5.2.2.2 Cohesive zone model

The cohesive zone model introduced by (Hillerborg, Mod er, & Petersson, 1976) has two basic implementations of the traction-separation laws used to model stiffness degradation after damage criteria are met, e.g., extrinsic, and intrinsic. Extrinsic formulation introduces cohesive elements, zones, or interfaces only after damage criteria are met thus making implementation difficult in practice. Intrinsic formulation introduces cohesive zones at the beginning of the analysis and requires handling the stiffness issues before the damage initiates. While intrinsic formulation suffers from issues with artificial compliance (predefined elements representing damage or crack location with artificially high stiffness and small thickness to limit their effect on the elastic behaviour), the extrinsic formulation requires handling the

strong discontinuity. The extrinsic formulation is compatible with eXtended finite element method (XFEM) and allows simulation (Ortiz, 1985) (Rots & Blaauwendraad, 1989) of the crack path development in the defined larger domain but at a higher computational cost. Selection between extrinsic and intrinsic implementation is important from the practical point of view and affects modelling procedure as well as interpretation of results.

Good agreement of the smeared approach (concrete damaged plasticity) with the cohesive zone model implemented via XFEM for crack growth simulation in RC beams without transverse reinforcement was shown in (Faron & Rombach, 2020). Different implementation of the intrinsic cohesive zone model is presented in (Sun & Zhu, 2021) for the simulation of sewer culvert failure. Four concrete models in LS-Dyna were compared in (Zhao, Lehman, & Roeder, 2021) and cohesive zone model was used for bond-slip modelling between steel and RC. RC beams with and without transverse reinforcement were tested and modelled in four-point bending test using cohesive zone model to simulate damage and capture the cracking behaviour of concrete with explicitly modelled reinforcement by (Kurumatani, Soma, & Terada, 2019). The method to predict crack width for the purpose of proper maintenance and prevention of damage due to reinforcement corrosion using a cohesive zone model is described by Yang et al in (Yang, Li, & Li, 2018). A mesoscale model for cracking of mortar induced by rebar corrosion using CZM is created by Xi et al in (Xi, S.Yang, & Li, 2018). Traction separation law for discrete strong discontinuity approach (DSDA) of to crack modelling was used compared in (Dias-da-Costa, Cervenka, & Graça-e-Costa, 2018) to smeared crack approach and general uncertainties of material were shown to affect both models but mesh sensitivity was not present for discrete crack modelling model.



Traction-separation laws: 1- bilinear, 2- exponential, 3- linear, 4- trapezoidal
 Initial behaviour within cohesive zone: a- initially rigid, b- initially elastic

Figure 5.1.3. Cohesive zone model: crack representation (left) and traction-separation laws (right)

Material parameters defined in the cohesive zone model require elastic stiffness matrix (for intrinsic formulation) and the damage definition, i.e., traction-separation law.

The elastic behaviour in three-dimensional problem (opening mode and two shearing modes are relevant deformations of the crack) is defined via stiffness matrix connecting tractions at the crack faces with strains:

$$\mathbf{t} = \begin{Bmatrix} t_n \\ t_s \\ t_t \end{Bmatrix} = \begin{bmatrix} K_{nn} & K_{ns} & K_{nt} \\ K_{ns} & K_{ss} & K_{st} \\ K_{nt} & K_{st} & K_{tt} \end{bmatrix} \begin{Bmatrix} \varepsilon_n \\ \varepsilon_s \\ \varepsilon_t \end{Bmatrix} = \mathbf{K} \boldsymbol{\varepsilon} \quad (9)$$

This implies that crack faces have predefined location in the model and are inserted in the mesh as the cohesive elements where the crack is expected a priori. Alternatively, cohesive zone elements can be distributed in the whole model as interfacial elements. In this case the care should be taken to the thickness definition and initial stiffness matrix \mathbf{K} values as to not affect the elastic response of the model with the artificial compliance. Similarly, the response outside of the elastic regime can be affected by overly rigid response or sudden activation of cohesive elements at the damage onset and can lead to convergence problem and numerical errors. Originally, Hilleborg defined the characteristic length of fracture process zone within isotropic materials as an intrinsic material property dependent on fracture energy G_f , young modulus E and damage initiation stress σ_{ini} .

$$l_{CZ} = E \frac{G_f}{\sigma_{ini}^2} \quad (10)$$

Which can be extended for different deformation modes in anisotropic materials where G_f can be mode I, II or III. Damage initiation is a material parameter required for CZM and can be obtained for different modes of deformation, opening -mode I, shearing along two directions- mode II and III. Mixed mode deformation requires handling damage criterion, e.g., maximum (Eq. (11)), quadratic (Eq. (12)) and can be based either on tractions or on strains.

$$\max\left(\frac{t_n}{t_{n,max}}, \frac{t_s}{t_{s,max}}, \frac{t_t}{t_{t,max}}\right) = 1 \text{ or } \max\left(\frac{\varepsilon_n}{\varepsilon_{n,max}}, \frac{\varepsilon_s}{\varepsilon_{s,max}}, \frac{\varepsilon_t}{\varepsilon_{t,max}}\right) = 1 \quad (11)$$

$$\frac{t_n^2}{t_{n,max}^2} + \frac{t_s^2}{t_{s,max}^2} + \frac{t_t^2}{t_{t,max}^2} = 1 \text{ or } \frac{\varepsilon_n^2}{\varepsilon_{n,max}^2} + \frac{\varepsilon_s^2}{\varepsilon_{s,max}^2} + \frac{\varepsilon_t^2}{\varepsilon_{t,max}^2} = 1 \quad (12)$$

After the criterion for damage initiation is met the damage evolution law is used to modify the tractions by scaling them with the damage variable D :

$$t_{damaged_{n/s/t}} = (1 - D)t_{n/s/t} \text{ and } D \in \langle 0, 1 \rangle \quad (13)$$

Damage evolution D can be defined either via displacement at failure or via fracture energy which are equivalent formulations and can have different shape, i.e., linear, bilinear, exponential see Figure 5.1.3, or defined as custom multilinear curve via tabular data. Damage evolution under mixed mode deformation around the crack (both opening and shearing present) can be defined via considering influence of different mode fractions in terms of energies or tractions:

$$m_I = \frac{G_I}{G_I + G_{II} + G_{III}}, m_{II} = \frac{G_{II}}{G_I + G_{II} + G_{III}}, m_{III} = \frac{G_{III}}{G_I + G_{II} + G_{III}} \quad (14)$$

5.2.2.3 Smearred cracking models outside plasticity theory

Smearred crack is imagined as a solid continuum and the cracked solid continuum response is modelled by stress-strain curves modification and elastic stiffness degradation (Rots & Blaauwendraad, 1989; Resende, 1987). The approach is valid for modelling microcracking of concrete and predicting the general direction of cracks that leads to the anisotropy of the material. The cracked concrete is here considered as the new material with updated stiffness and anisotropic properties. Thus, orthotropic stiffness matrix is used in the constitutive equations.

Compression field theory (CFT) and Modified CFT are the theoretical works behind the smeared crack model implementation within DIANA commercial software (referred to as total strain-based crack model). Modified compression field theory was developed for tension and compression stress states of reinforced concrete panels. Later, the modified CFT was extended to the confinement problems, namely the triaxial stresses and lateral expansion. The triaxiality strength envelope criterion of Mohr-Coulomb was used. The theory operates on averaged strains to describe the crushing and cracking in concrete.

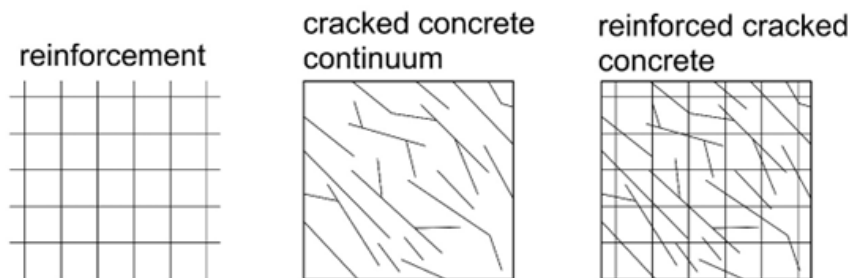


Figure 5-5: Schematic assumptions of the smeared crack model for concrete.

Compression field theories (CFT) are applied to predict the shear response of RC beams by (Guo, Dong, Bastidas-Arteaga, & Gu, 2021). The smeared crack approach is also applied in the works of e.g., (Gomes, et al., 2020) to evaluate shrinkage and temperature induce cracks, and by (Castaldo, Gino, & Mancini, 2019) to compare different safety formats within non-linear FEA using ATENA software for the simulation of RC beams in bending. The smeared crack model (either fixed or rotated) as implemented in ATENA software is compared with a discrete strong discontinuity approach by Dias da Costa (Dias-da-Costa, Cervenka, & Graça-e-Costa, 2018) and mesh sensitivity as well as high uncertainties in crack width estimation are pointed for the smeared approach. Machine learning techniques were employed to prevent convergence issues within CFT on the example of generic RC beam elements by (Hernández-Díaz, Pérez-Aracil, Casillas-Perez, Pereira, & Salcedo-Sanz, 2022).

The cracking caused by expansion of volume due to corrosion of rebar is modelled using the smeared crack model in (Liu & Su, 2018) and the critical displacement due to expansion is shown to be ruled by mechanical material properties of concrete rather than environmental parameters influencing corrosion. Disturbed stress field model, an extension of the modified compression field theory was proposed by (Vecchio & Collins, 1986) was utilized in the punching shear problem of RC slabs by (Goh & Hrynyk, 2020). Total strain crack model with bond-slip curve from Model Code integrated into steel stress-strain law was proposed in (Terán & Haach, 2018) and applied to simulation of RC slab laboratory experiments. A new model for quasi-brittle materials that has many parallels to smeared fixed or rotating crack approach is presented in (Cervera, Tesei, & Ventura, 2018). Model of caisson foundations in the soil were made using compression field theory within VecTor2 software by (Guner, 2023).

Total strain-based crack model

The stress-strain relation is used for ease of implementation within FEM. Three approaches: rotating, fixed, and switching direction crack models can be distinguished. The rotating crack model orients the crack direction according to the principal stresses in each step and therefore the tangential stresses along the crack are not present. However, only one crack can be present at a given time step as it is determined by the maximum principal stress. The fixed-crack model assumes crack direction based on the principal stress directions at the onset of the crack and 'remembers' it during the subsequent crack propagation while tangential stresses to the crack propagation direction are present. The localization of the crack within the total strain crack model is not determined and is as accurate as the mesh density since the cracked versus non-cracked state is determined at the integration points. Total strain crack model was

used to simulate concrete failure in the RC column and foundation connection under cycling loading by (Nascimbene & Bianco, 2021). RC beams 2D models are built in (Wani, Khan, & Vemuri, 2022) to compare how different parameters (amount of steel, shear retention factor, beam depth) affect the numerical results of total strain-based crack model in DIANA software. Structural behaviour of the RC beams subjected to frost is modelled via a multiscale scheme (2D heat transfer in mesoscale and 3D structural analysis for macroscale) using total strain-based model (Wang, Hayashida, Zhang, Gong, & Ueda, 2020). A multi-physics framework was simulating the hygro-thermo-mechanical behaviour of RC slabs (shrinkage, cracking) using the smeared multi-directional fixed cracking model in DIANA FEA software (Carvalho, et al., 2020). Several RC beams with varying hole geometry were modelled with a fixed crack model (SBeta model in ATENA) to compare safety formats non-linear FEA (Castaldo, Gino, & Mancini, 2019).

Fixed crack (smeared crack) model is used with a new finite element formulation in (Chang, Lee, Carr, & Dhakal, 2019) for simulation of RC shear walls. A comparison of three commercial software using fixed-crack models with shear retention on force-displacement curves and crack patterns from several experimental specimens is analysed by (Castaldo P., Gino, Bertagnoli, & Mancini, 2018). Capacity loss due to corrosion in bridge girders was modelled by (Osmolska J., Kanstad, A.N., & G, 2022) using a rotating crack approach and the shear performance was found to be very sensitive to material parameters. Caisson foundations strengthening method modelling methodology with focus on reinforcement details was made within smeared cracking approach by (Guner, 2023).

The smeared crack model is implemented in commercial software, e.g., DIANA (total strain-based crack), ABAQUS (elastic cracking model for concrete), and ATENA (SBeta model).

The fixed-crack model requires the definition of the shear stresses (e.g., shear retention) that remain in the model due to the crack direction not being oriented with the direction of principal stresses in the current step of the analysis. On the other hand, the rotating crack model avoids this problem but does not allow for multiple crack definition which can be critical to properly simulating many problems. The rotating crack model requires definition of threshold angle, i.e., an angle based on the principal stress direction change that adjusts the cracking plane direction in each step of the analysis.

The principal stress space is used to evaluate the principal directions of the strains n,s,t and establish general crack direction, where n is normal, and s and t are tangential.

$$\begin{bmatrix} \sigma_{nn} \\ \sigma_{ss} \\ \sigma_{tt} \\ \sigma_{ns} \\ \sigma_{st} \\ \sigma_{tn} \end{bmatrix} = \begin{bmatrix} E_{nn} & E_{ns} & E_{nt} & 0 & 0 & 0 \\ E_{ns} & E_{ss} & E_{st} & 0 & 0 & 0 \\ E_{nt} & E_{st} & E_{tt} & 0 & 0 & 0 \\ 0 & 0 & 0 & G_{ns} & 0 & 0 \\ 0 & 0 & 0 & 0 & G_{st} & 0 \\ 0 & 0 & 0 & 0 & 0 & G_{nt} \end{bmatrix} \begin{bmatrix} \varepsilon_{nn} \\ \varepsilon_{ss} \\ \varepsilon_{tt} \\ \varepsilon_{ns} \\ \varepsilon_{st} \\ \varepsilon_{tn} \end{bmatrix} \quad (15)$$

The stress is then updated in the coordinate system aligned with crack (either fixed or rotating). Stiffness matrix is updated either as tangent or secant:



$$D_{tangent} = \begin{bmatrix} D_{nn} & D_{n\theta} \\ D_{\theta n} & D_{\theta\theta} \end{bmatrix}, \quad D_{secant} = \begin{bmatrix} \bar{E}_1 & 0 & 0 & 0 & 0 & 0 \\ 0 & \bar{E}_2 & 0 & 0 & 0 & 0 \\ 0 & 0 & \bar{E}_3 & \bar{G}_1 & 0 & 0 \\ 0 & 0 & 0 & 0 & \bar{G}_2 & 0 \\ 0 & 0 & 0 & 0 & 0 & \bar{G}_3 \end{bmatrix} \quad (16)$$

Where D_{nn} is the tangent stiffness sub matrix (3x3) for normal components and $D_{\theta\theta}$ is tangent stiffness matrix for shear components (3x3 and diagonal). $D_{n\theta}$ and $D_{\theta n}$ matrices are normal-shear stress coupling terms and can be non-zero in the fixed crack approach, modelling so called shear retention with different assumed law. Secant stiffness matrix is diagonal and can represents 3D orthotropic material with zero Poisson ratios in every direction (i.e., no lateral deformations caused by a deformation applied on a given direction). The procedure for updating stiffnesses is outside theory of elasticity and does not allow this approach to be combined with other constitutive models. (WILLAM & WARNKE, 1975).

Smearred cracking models based on anisotropic materials model with degraded stiffness require careful choice of shear retention factor (fixed crack), threshold angle (rotating models), and Poisson ratio. Shear retention factor is commonly chosen due to the inability of the smeared crack model with fixed crack to reproduce the aggregate interlocking causing shear resistance or shear friction. Most model introduce shear stiffness reduction with constant, linear or other law defining β_s :

$$G = (1 - \beta_s)G_0, \quad \beta_s \in \langle 0, 0, 0, 5 \rangle \quad (17)$$

According to (Rots & Blaauwendraad, 1989), fixed-crack concept results in over stiff response despite adjusting shear retention factor, while rotating crack concept results in a flexible response. The over-stiff response is caused by stress-locking, that is found fundamental to the smeared softening cracking approaches that do not include discontinuity.

5.2.2.4 Fracture-plastic model

This model was developed by (Červenka & Papanikolaou, 2008) and is implemented within the commercial software (ATENA). Orthotropic model for smeared rotating crack with Rankine criterion is used in tension while plasticity theory is applied for compression/concrete crushing with Menetrey-Willam yield criterion. The separation of the models is based on strain decomposition into elastic, plastic, and fracture strains:

$$\dot{\epsilon}_{ij} = \dot{\epsilon}_{ij}^e + \dot{\epsilon}_{ij}^p + \dot{\epsilon}_{ij}^f \quad (18)$$

Stresses are evaluated using elastic strains and stiffness matrix D while plastic and fracture strains are evaluated separately based on the multi-surface plasticity concept with plastic and fracture potential surfaces f:

$$\dot{\sigma}_{ij} = D_{ijkl} \left(\dot{\epsilon}_{kl} + \dot{\epsilon}_{kl}^p + \dot{\epsilon}_{kl}^f \right), \quad \dot{\epsilon}_{ij}^p = \dot{\lambda}^p \cdot \frac{\partial f^p}{\partial \sigma_{ij}}, \quad \dot{\epsilon}_{ij}^f = \dot{\lambda}^f \cdot \frac{\partial f^f}{\partial \sigma_{ij}}$$

The model is intended to use for plain and reinforced concrete structures.

Fracture-plastic model was combined with a chloride ingress model to predict serviceability based on crack width for ageing structures (Hájková, Šmilauer, Jendele, & Červenka, 2018). Corroded reinforced columns under cycling loading were modelled by (El-Joukhadar, Dameh, & Pantazopoulou, 2023). RC beams were modelled by (Yang, Wang, Yang, & Wang, 2023) to check the influence of the bond-slip on the capacity. A comparison of concrete damaged plasticity model from ABAQUS and plastic-fracture model as implemented in ATENA for the punching shear analysis in RC slab is shown in (Panahi & Genikomsou, 2022). RC columns with strengthening were modelled using plastic-fracture model by (Paz, Marques, & Ruas, 2022).

5.2.2.5 Material models in codes and standards

Tensile and compressive stress-strain curves (constitutive models) of concrete in uniaxial conditions are defined in several design codes and can be applied with different compatible numerical models for FEA as material parameters when experimental curves are not available. Short term compression stress-strain curves from EC2-1992-1-1, CEB-FIP 1990 and FIB 2010 are depicted in Figure 5-6.

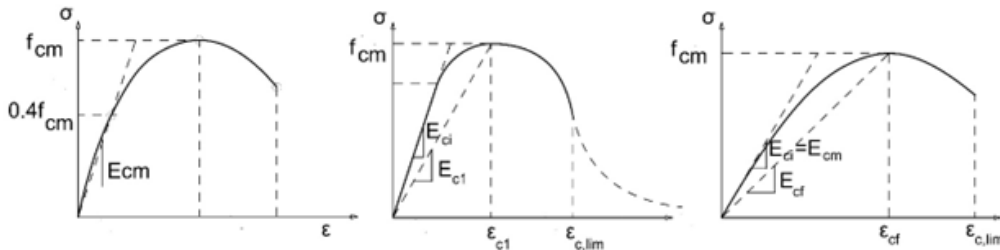


Figure 5-6: Compression stress-strain curves in uniaxial load defined by EC2-1992-1-1 (CEN, 2004)(left), CEB-FIP 1990 (centre), and FIB 2010 (right).

The curves for EC2 and FIB 2010 relations is approximated until the point of limiting strain $\epsilon_{c,lim}$ by the formula:

$$\sigma_c = -\frac{1.05 \frac{E_{ci}}{E_{c1}} \frac{\epsilon_c}{\epsilon_{c1}} - \left(\frac{\epsilon_c}{\epsilon_{c1}}\right)^2}{1 + \left(\frac{E_{ci}}{E_{c1}} - 2\right) \frac{\epsilon_c}{\epsilon_{c1}}} f_{cm} \quad (19)$$

Here, the tangential stiffness E_{ci} and the secant stiffness $E_{c1}=E_{cf}$ are defined. The descending branch can be approximated either as a straight line or as a softening curve. The bilinear (rectangular stress distribution) or parabolic stress-strain relationships are allowed for design of cross-sections. Stress-strain relationships are scaled for the case of confined concrete (effective lateral compressive stress is present), e.g., when crossties are present and spaced closely enough.

CEB-FIP model Code from 1990 defines tensile stress-strain curves for uncracked concrete as non-linear elasticity model (multilinear elasticity) and stress-displacement curves for crack opening.

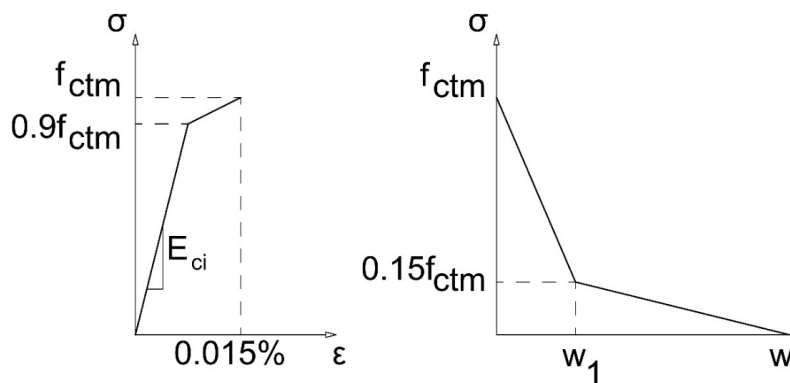


Figure 5-7: Tension stress-strain and stress-crack displacement curve from CEB-FIP 1990 Model Code.

5.2.2.6 Multi-scale models

For modelling in detail specific mechanisms within reinforced concrete and capturing their micro or mesoscale mechanics and its influence on the macroscale structural behaviour, the multi-scale modelling is applied. Most commonly, the different damage mechanisms due to environmental exposure (corrosion, chloride ingress, freeze and thaw) and its dependence on the concrete composition and reinforcement placement is investigated.

A mesoscale model (rigid body spring model) for freeze and thaw damage using Rigid Body Spring model to predict the tensile and compressive behaviour was described in (Wang, Gong, Zhang, Wang, & Ueda, 2019). The model is used to develop frost damaged concrete constitutive properties for application in FEA. Microscale model for multiphysics based freeze and thaw damage in the representative volume element was developed to predict degradation of the mechanical properties based on the mix components and environmental factors (Peng, Qiu, & Jiang, 2022). A multiscale approach to crack pattern modelling in concrete affected by the heterogeneity of aggregate, cement matrix, and interfacial transition zones using stiffness degradation on the macroscale was applied by (Zhong, Zhuang, Shiyang, & Zhou, 2021).

5.2.2.7 Bond-slip model

Bond-slip relation describes interaction of the concrete and reinforcing steel and can relate both to the interface/surface contact properties as well as fracture of concrete around reinforcement. The complex nature of the interaction results from different mechanical properties of steel and concrete and different mechanisms involved, i.e.:

- chemical adhesion,
- surface friction,
- mechanical contact/locking

Ground research work on constitutive relation modelling of steel-concrete bond behaviour was published by (Shima, Chou, & Okamura, 1987). Bond-slip relations were found to depend on the location along the bar, boundary conditions, embedment length, bar diameter, and concrete compressive strength among others.

Delamination is modelled with the phenomenological approach using shear-displacement curves, that can be defined as monotonic or include softening and are commonly based on the experimental data, see Figure 5-8.

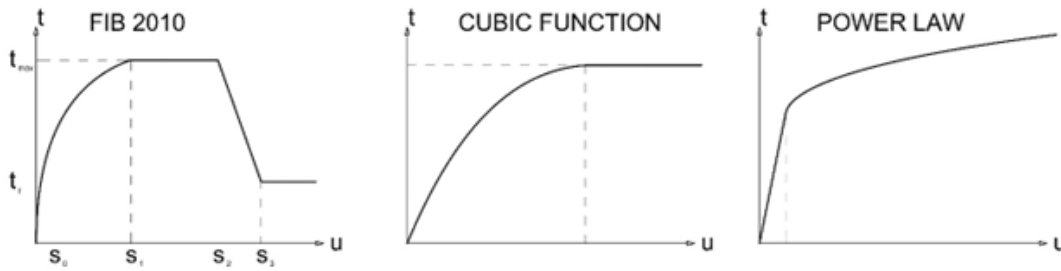


Figure 5-8: Bond-slip relations from FIB Model Code 2010, the cubic function of Dorr and Power law from Nowakowski (Chen & Chen, 1975).

Those phenomenological models assume certain mechanism occurring at the concrete-reinforcement interface and need to be chosen with care. When the microcracking of concrete occurs around the rebar in the initial loading stage the maximum capacity of shear load transfer is obtained and the delamination leads to activation of friction and direct transmission of force in contact that can either cause stress plateau, hardening or drop toward residual capacity. The mechanism is dependent on the geometry of the concrete, volume of the concrete around the rebar, rebar shape, presence of transverse reinforcement, and material properties of all elements.

Bond slip model is investigated in (Hasan, Qasem, Muhamad, & Mutafi, 2022) to model concrete to steel interface in the connection between precast RC wall panels and properly simulate shear-slip behaviour. It is common t

5.2.2.8 Time dependent long-term effects models: creep

Creep behaviour is defined as strain increase over time under sustained constant stress applied. Creep is influenced by relative humidity, dimensions of concrete structure, and concrete mix composition as well as time of application of the permanent loading with respect to the concrete maturity. The creep for concrete is defined within codes via a coefficient φ , a ratio of the long-term strain ε_{cc} at time t to the initial strain ε_{ci} at time $t_0=28$ days (elastic). The initial elastic strain is inversely proportional to the tangent elastic modulus of 28 days concrete E_{ci} and proportional to the applied stress σ_c .

$$\varphi(t, t_0) = \frac{\varepsilon_{cc}(t, t_0)}{\varepsilon_{ci}} = \frac{\varepsilon_{cc}(t, t_0)}{\sigma_c(t_0)} E_{ci}, \quad \sigma_c < 0.45 f_{ck} \quad (20)$$

Non-linear creep occurs after certain value of permanent load is exceeded (45% of the characteristic compressive strength limit f_{ck} according to the EC2). For $t=\infty$, the final creep (maximum deformation) coefficient is obtained.

$$\varphi_{nl}(t, t_0) = \varphi(t, t_0) \exp\left(1.5 \left(\frac{\sigma_c}{f_{ck}} - 0.45\right)\right), \quad \sigma_c > 0.45 f_{ck} \quad (21)$$

For special cases of loading, creep recovery and the influence of other nonlinearities on the creep behaviour, the numerical viscoelastic models are applied. The most popular rheological model (rate dependent) is Maxwell model.

5.2.2.9 Software for non-linear RC simulation

The most used software identified within scientific literature in the last six years that allows for non-linear simulation of the reinforced concrete is listed below:

- DIANA: total strain-based crack, plasticity-crack model
- ABAQUS: damaged plasticity model, elastic-cracking model, elastic-plastic
- ATENA: orthogonal crack model, plastic-fracture model
- COMSOL, Ottosen concrete model and Mazars damage model
- ANSYS, plastic damage model SOLID65
- SOFISTIK, no clear information of the applied approach in material modelling
- LS-DYNA: continuous surface cap model, damaged plasticity model,
- Response/ Response 2000
- VecTor, VecTor2, smeared rotating crack
- ADINA

Unlicensed and self-developed software without open-source license was not included in the list.

5.2.3 Material modelling of reinforcing steel

Reinforcing steel, hereon referred to as rebars, is assumed to behave like a ductile isotropic material that can be well described within classic plasticity theory with associated flow rule (plastic strain rate vector is oriented normal to the plastic potential surface). Typical stress-strain relationship from a uniaxial tensile test of steel dog bone specimen is used to obtain the material characteristics, see Figure 5-9 on the left.

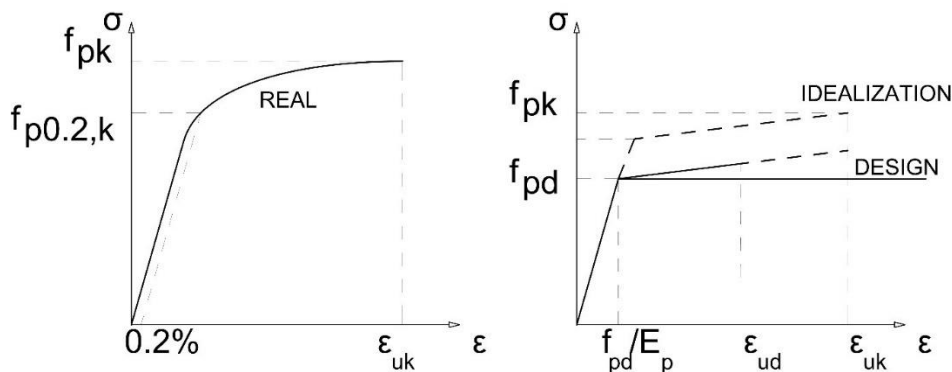


Figure 5-9: Stress-strain relations for rebars (left) and model assumption (right).

The characteristic and design values can be obtained based on the material tests and idealized elastic-plastic model is the simplest nonlinear model for rebars, see Figure 5-9 to the right. The von Mises criterion is typically chosen for the yield function in which the onset of plasticity is only dependent on deviatoric stresses, i.e., plasticity is independent of the hydrostatic stress. Plasticity occurs when the yield function, f , is equal to zero, viz.

$$f = \sigma_{Mises} - \sigma_y \quad (22)$$

where σ_y is the uniaxial yield stress and σ_{Mises} is the equivalent von Mises stress which can be stated in terms of the stress tensor as

$$\sigma_{Mises} = \sqrt{\frac{1}{2} \left[(\sigma_{11} - \sigma_{22})^2 + (\sigma_{22} - \sigma_{33})^2 + (\sigma_{33} - \sigma_{11})^2 + 6(\sigma_{12}^2 + \sigma_{23}^2 + \sigma_{31}^2) \right]} \quad (23)$$

Typically, rebar steel is modelled as either perfect plastic or with linear hardening, as seen in Figure 5-9. In a perfect plastic material, the yield stress is constant while for linear hardening the yield stress evolves with plastic strains as

$$\sigma_y = \sigma_0 + H_r \lambda^p \quad (24)$$

Where σ_0 is the initial uniaxial yield stress, H_r is the hardening modulus and λ^p is the plastic multiplier. Plastic strains evolve according to a plastic flow rule, i.e., the yield function is used as a plastic potential viz.

$$\dot{\varepsilon}_{ij}^p = \dot{\lambda}^p \frac{\partial f}{\partial \sigma_{ij}} \quad (25)$$

Note that combination of associated plastic flow and a pressure independent yield surface leads to incompressible plastic flow. The Cauchy stress tensor is given by Hooke's law

$$\dot{\sigma}_{ij} = D_{ijkl} \left(\dot{\varepsilon}_{kl} - \dot{\varepsilon}_{kl}^p \right) \quad (26)$$

where D_{ijkl} is the elastic stiffness tensor and $\dot{\varepsilon}_{kl}$ is the total strain rate tensor.

5.2.4 Material modelling of prestressing steel

This subsection will be included in the revision of the document.

5.2.5 Modelling of tension stiffening

Tension stiffening is caused by the mechanical bond, mainly due to the rib interaction between the embedded rebars and the surrounding concrete in between cracks formed (Marti, Alvarez, Kaufmann, & Sigrist, 1998; Russo & Romano, 1992). The effect reduces the deformation capacity of a structure compared to when the rebars are assumed to uptake the tensile forces alone, and is a paramount effect to obtain correct stiffness and failure mode of a structure (Mata-Falc3n, Tran, Kaufmann, & Navr3til, 2018). The effect is conceptually visualized in Figure 5-10, at which Figure 5-10 a) represents the strain distribution of a cracked RC tie. It is noticed that the steel strains are at its maximum at the cracked face, i.e. as F/EsAs, whereas the concrete strains are null at this location since all tensile forces are assumed carried by the rebar at the crack. The steel strains reduces thus further away from the cracked face due to the bond interaction between rebar and concrete, reaching its minimum at the symmetry section whereas the concrete strains reaches its maximum. The mean strains of the RC tie is therefore smaller than the steel strains at the cracked face and is what is referred to as the tension stiffening effect as indicated in Figure 5-10 b).

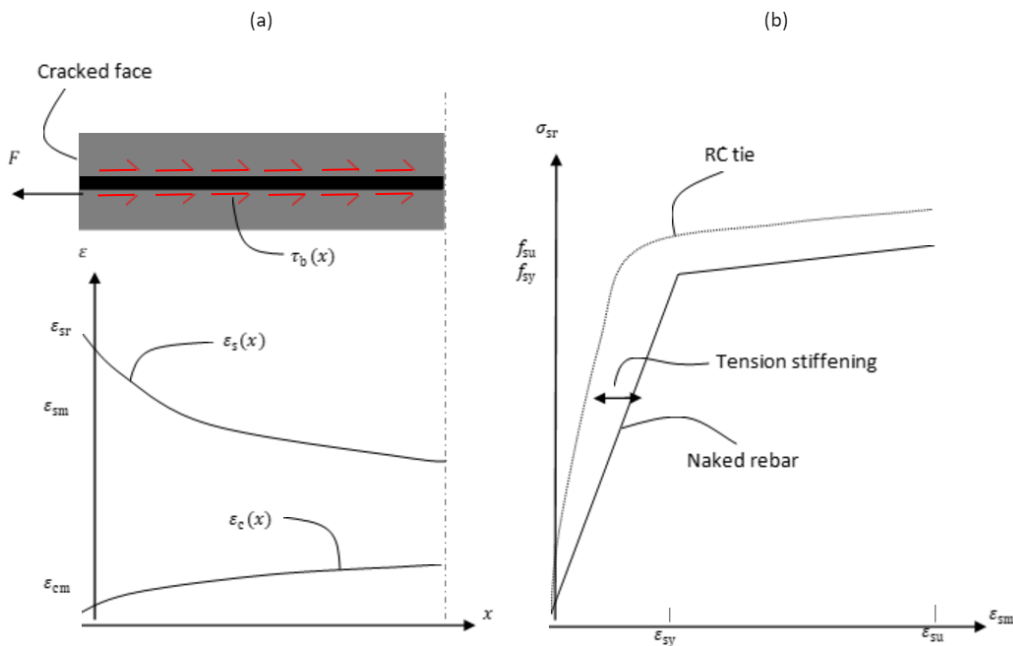


Figure 5-10: Tension stiffening effect. (a) Strain distribution for rebar and concrete of a cracked RC tie. (b) Stress strain response of a RC tie.

The effect is normally modelled by either of the following model compositions

1. Tension chord models for the embedded rebar elements combined without tension softening of the concrete elements (Kaufmann & Marti, 1998; Tan, Hendriks, Geiker, & Kanstad, 2019).
2. Local bond-slip curves combined with naked rebar behaviour and tension softening of concrete elements (Cervenka, Rimkus, Gribniak, & Cervenka, 2022).
3. Naked rebar behaviour combined with tension softening of relatively small concrete elements to obtain strain localization over a row or column of elements (Hendriks, de Boer, & Belletti, 2016).
4. Modification of tension softening behaviour in concrete elements with embedded rebar elements (Stramandinoli & Rovere, 2008).

The subsequent chapters deal with how reinforcement corrosion can be accounted for through the tension stiffening effect.

5.3 Modelling of reinforcement corrosion

5.3.1 General

Carbonation and chloride induced corrosion are the two main corrosion types occurring in RC structures and are the two mechanisms that will be addressed in this study. Carbonation induced corrosion causes uniform corrosion and affects the bond between concrete and steel over a considerable length of the rebars, while chloride induced corrosion causes local or so-called pitting corrosion of rebars. The following focuses on how both corrosion mechanisms affect the mechanical behaviour of RC ties, and how this can be accounted at material level when performing NLFEA.

5.3.2 Pitting corrosion

5.3.2.1 Mechanical behaviour of pitting corroded rebars

The deterioration caused by pitting corrosion is replicated according to (Haefliger, 2022), and is derived in a mechanical sound manner by considering a naked rebar with a certain length l having an uncorroded part with length l_{uc} and a corroded part with length l_c . The cross-sectional area of the rebar A_s is thus reduced over the length l_c as

$$A_{s,c} = (1 - \zeta)A_s \quad (27)$$

Where

$$\zeta = \frac{A_{s,lost}}{A_s} < 1 \quad (28)$$

By equilibrium,

$$F = A_s \sigma_{s,uc} = A_{s,c} \sigma_{s,c} = (1 - \zeta)A_s \sigma_{s,c} \quad (29)$$

This means that the total elongation of the rebar can be decomposed to

$$u_{tot} = \frac{F}{A_{s,c} E_s} l_c + \frac{F}{A_s E_s} l_{uc} = \varepsilon_{s,c} l_c + \varepsilon_{s,uc} l_{uc} \quad (30)$$

By inserting for Eq. (27) in (29) the relation between the stresses for the corroded and uncorroded part becomes

$$\sigma_{s,c} = \frac{\sigma_{s,uc}}{(1 - \zeta)} \quad (31)$$

The rebar force at yielding is thus limited by

$$F_y = A_{s,c} f_{sy} = (1 - \zeta)A_s f_{sy} = A_s \sigma_{sy,uc} \quad (32)$$

And at failure by

$$F_u = A_{s,c} f_{su} = (1 - \zeta)A_s f_{su} = A_s \sigma_{su,uc} \quad (33)$$

At which the steel stresses at yielding of the rebar for the uncorroded part are limited to

$$\sigma_{sy,uc} = (1 - \zeta)f_{sy} \quad (34)$$

And at ultimate to

$$\sigma_{su,uc} = (1 - \zeta)f_{su} \quad (35)$$

Consequently, the total elongation of the rebar at ultimate is reduced since

$$\varepsilon_{su,uc} = \varepsilon_s(\sigma_{su,uc}) < \varepsilon_s(f_{su}) \quad (36)$$

The critical cross-section loss ζ_{crit} can be found by exerting the following equilibrium of the uncorroded and corroded part

$$A_s f_{sy} = (1 - \zeta_{crit}) A_s f_{su} \quad (37)$$

$$\zeta_{crit} = 1 - \frac{f_{sy}}{f_{su}}$$

Cross-sectional losses larger than ζ_{crit} implies that the uncorroded part remains elastic when the corroded part ruptures. This means that plastic strains localise in the corroded part and that the total elongation at ultimate, or more rigorously speaking the deformation capacity, is drastically reduced. The material models for uncorroded and corroded rebars have been visualized generically in Figure 5-11.

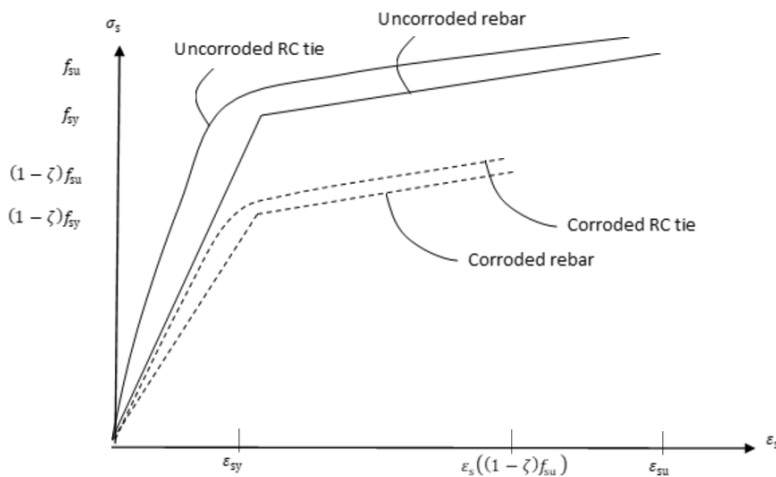


Figure 5-11: Generalized material models for uncorroded and corroded rebars

The authors (Cairns, Plizzari, Du, Law, & Franzoni, 2005; Du, Clark, & Chan, 2005) proposed empirical adjustments for ζ as a function of the yield stress, ultimate stress and strain, degree of corrosion, and whether it is uniform or pitting corrosion governing the deterioration of the rebar. The approach was later adopted by (Osmolska J., Kanstad, A.N., & G, 2022) to predict the behaviour of deteriorated RC structures subjected to pitting corrosion applying NLFEA.

5.3.2.2 Mechanical behaviour of pitting corroded RC ties

The formulation for pitting corroded rebars is applicable for modelling tension stiffening according to compositions 2-4 proposed in subchapter 5.2.5. However, the main issue with these methods is that they are computationally time inefficient for relatively large FE models and for such infrastructures of interest in this project, since they require rather fine mesh to obtain strain localization and/or additional bond-slip formulations. At the other end of the scale is the approach that models tension stiffening according to composition 1 in subchapter 5.2.5, which offers more computationally time efficient method in comparison. This can be accredited to the model composition allowing for the use of relatively large finite elements and coarse meshes, while accounting for tension stiffening via the analytical tension chord model. Furthermore, it was shown by (Haefliger, 2022) that a tension chord model can be adjusted in a

relatively simple manner to account for pitting corrosion. The outcome was the Corroded Tension Chord Model, which still is a fully mechanical sound model without any empirical adjustments what so ever. The generalized behaviour of such models are conceptually visualized in Figure 5-11, and offers a pragmatic yet mechanically convincing method of accounting for the tension stiffening behaviour of pitting corroded RC ties to perform NLFEA.

5.3.3 Uniform corrosion

Carbonation induced corrosion is caused by the ingress of carbon dioxide into concrete, which further reacts with calcium hydroxide of the cement paste. This causes mainly uniform corrosion and affects a considerable length of the reinforcing steel. The resulting corrosion products leads to volume expansion and consequently spalling of concrete cover. The corrosion rate is rather low leading to a diameter loss of typically 0,01 mm/year (Haefliger, 2022).

The mechanical consequence of uniform corrosion is that the bond between embedded rebars and surrounding concrete is deteriorated. This can first and foremost risk in brittle anchorage failures of rebars and will in addition reduce the tension stiffening effect of RC structures. However, it was argued by (Haefliger, 2022) that the latter affects the deformation capacity negligibly at least in comparison with strain localisation effects caused by pitting corrosion. In any case, the uniform corrosion can be accounted for by adjusting the bond-slip parameters if a bond-slip model and/or a tension chord model is applied in NLFEA.

5.4 Modelling of damaged prestressing

This subsection will be included in the next revision of the document.

5.5 Modelling of ASR

5.5.1 Introduction: Material characteristics of ASR-affected concrete, and structural consequences

On the concrete material scale, the most prominent effects of alkali-silica reaction are expansions and changes in material behaviour, e.g., reduction in tensile strength and modulus of elasticity (Swamy & Al-Asali, 1988), (Giaccio G. , Zerbino, Ponce, & Batic, 2008), (Smaoui, Bissonnette, Bérubé, Fournier, & Durand, 2005), (Esposito, Anac, Hendriks, & Copuroglu, 2016) and (Kongshaug S. , et al., 2020). The expansion and the material degradation are caused by the swelling of the ASR-gel by water absorption at discrete reaction sites in the reactive aggregates, leading to pressure in the gel, and tensile stresses in the surrounding cement paste. As a result, a dispersed network of microcracks develops, with its extent and characteristic orientation related to the expansion and degradation of the material (Giaccio, Torrijos, Tobes, Batic, & Zerbino, 2009) and (Kongshaug S., et al., 2020). On the structural level, the most noticeable signs of ASR are surface cracks and displacements leading to closing of expansion joints in bridges (Jensen, 2004) and inclined columns. Large structural through-cracks up to 6 mm in Elgeseter Bridge in Norway are caused by ASR (Dr. Ing. A. Aas-Jakobsen AS, 2013) (Kongshaug, Hendriks, Kanstad, & Markeset, 2022).

Material deformations that are not from stress, such as thermal dilation/contraction and drying shrinkage, induce stress/load effects. From expressions for the evolution of shrinkage strain, e.g. in Eurocode 2 (CEN, 2004), one finds that shrinkage strain is one order smaller than the ASR expansion observed in experimental investigations, cf. with the experimental studies cited in the previous paragraph. The ASR-induced expansions in the mentioned studies are also one order greater than thermal strain even for large temperature variations ($\Delta T=40$ °C).

In contrast to thermal expansion, expansion owing to ASR applies only to the concrete. Reinforcement bars will therefore have a restraining effect on the expanding concrete. This means that tensile stresses develop in the reinforcement and compressive stresses in the concrete; this is like the effect of shrinkage but with the opposite sign. In addition to the local expansion incompatibility between concrete and steel, differential ASR expansions/strains at the structural level might occur because of moisture gradient as experimentally investigated by (Multon, Seignol, & Toutlemonde, Structural behavior of concrete beams affected by alkali-silica reaction, 2005), where it was shown that a vertical moisture gradient gave rise to a vertical variation in the ASR-induced expansion. Besides, the rate of ASR, and thus the rate of expansion, is dependent on temperature, so temperature variations may cause spatial variations in the ASR-induced expansion. From heat and moisture transport characteristics in concrete, it can be argued that temperature variations are important for massive concrete structures such as dams, while moisture variations are more important for slender structures such as bridges (Ulm, Coussy, Kefei, & Larive, 2000) and (Comi, Kirchmayr, & Pignatelli, 20112). In this way, temperature and moisture may play an important role in the spatial variation of ASR expansion.

In contrast to shrinkage and thermal strain, the ASR expansion is anisotropic, i.e., different in each direction. One distinguishes between two types of expansion anisotropy: intrinsic anisotropy, and stress-induced anisotropy. The intrinsic is explained by two reasons (Smaoui, Bérubé, Fournier, & Bissonnette, 2004): 1) porous and weak zones under the aggregates due to trapped water, resulting in lower resistance along the casting plane to the expansive pressure developed by ASR, and 2) preferred orientation of elongated aggregates along the casting plane, creating higher areas of expanding aggregates along this plane. Although the chemical reaction (ASR) is stress-independent, the expansion is highly influenced by stress. If the concrete is uniaxially loaded in compression during ASR development, the expansion is reduced in the load direction, where the compressive stress necessary to stop the expansion ranges between 3 and 10 MPa (Herrador, Martínez-Abella, & Rabuñal Dopico, 2008). Consequently, an anisotropic stress state causes anisotropic expansion. Four expansion behaviours can be identified among experimental investigations for compressed concrete with at least one direction free of stress:

1. total transfer of expansion to the stress-free directions, i.e., volumetric expansion is preserved (Larive, 1997) (Multon & Toutlemonde, 2006) (Gautam, Penesar, Sheikh, & Vecchio, 2017); partial transfer (Berra, Faggiani, Mangialardi, & Paolini, 2010) (Kagimoto, Yasuda, & Kawamura, 2014) (Liaudat, Carol, López, & Saouma, 2018);
2. no or negligible transfer to the stress-free directions (Jones & Clark, 1996) (Gravel, Ballivy, Khayat, Quirion, & Lachemi, 2000);
3. the expansions in the stress-free directions are reduced (Ahmed, M.A, Burley, & Rigden, 1999) (Dunant & Scrivener, 2012).

Because the expansion is related to the extent and orientation of micro cracks, an anisotropic expansion corresponds with an anisotropic degradation of the material (Kongshaug S., et al., 2020). Both the stiffness (measured modulus of elasticity) and the tensile strength are reduced with increasing expansion.

Considering the magnitude ASR expansion, the expansion incompatibility between concrete and reinforcement, and the expansion incompatibility between structural parts caused by temperature and moisture variations, it follows that ASR may cause significant additional stresses/load effects. In design, deformations due to temperature and shrinkage are often considered in separate load cases, and the load effects are superimposed with the load effects from external actions. Load effects due to imposed deformations are highly dependent on the stiffness of the system, where in general, greater stiffness leads to larger load effects. Therefore, when imposed deformations are analysed, it is important that the structural model can represent the true rigidity. For instance, creep and cracking will highly affect the structural stiffness, and if these phenomena are present, they should be accounted for in the concrete

material model. In addition, the influence of reinforcement on structural stiffness must be accounted for. Accounting for these material effects results in non-linear material equations, which necessitates a non-linear solution procedure.

The multi-scale nature of ASR is reflected in the huge diversity in material models, ranging from the chemical to the concrete scale. An overview of existing models is given in the review paper of (Esposito & Hendriks, Literature review of modelling approaches for ASR in concrete: a new perspective, 2019), where the models are classified based on their starting scale of modelling. The models are also assessed to which extent they can be extended to structural analysis. In a structural analysis of large-scale reinforced concrete structures, such as bridges and dams, a model on the concrete scale must be sought. This means that the constituents at the subscale of concrete are not explicitly modelled, and the subscale physics is included in a smeared or averaged fashion. Only these types of models are considered in the following.

5.5.2 Modelling ASR-induced expansions

In the following, Voigt notation is used for stress σ and strain ϵ , where bold-faced letters are vectors.

The most common way to incorporate ASR-induced expansions in structural analysis is to consider the expansion as an imposed deformation/strain (Courtier, 1990) (May, Wen, & Cope, 1992) (Wen, 1993) (Léger, Côté, & Tinawi, 1996) (Saouma & Perotti, 2006) (Multon, Seignol, & Toutlemonde, Chemomechanical assessment of beams damaged by alkali-silica reaction, 2006) (Kongshaug, Larssen, Hendriks, Kanstad, & Markeset, 2021) (Kongshaug, Hendriks, Kanstad, & Markeset, 2022). In this way, the total strain of the concrete is decomposed into a mechanical strain ϵ^m , and an imposed strain ϵ^i :

$$\epsilon = \epsilon^m + \epsilon^i \quad (38)$$

The mechanical strain ϵ^m is caused by stress, and it can be further decomposed to account for cracking or creep, see Section 5.2.2 for more information. On the other hand, imposed strain is not caused by stress but by other physical quantities; the most familiar for concrete are thermal dilation/contraction (temperature dependent) and drying shrinkage (moisture dependent). Introducing the effect of ASR as an imposed deformation, the total imposed strain is decomposed in three parts: thermal strain ϵ^T , shrinkage strain ϵ^{sh} , and ASR strain ϵ^{asr} ;

$$\epsilon^i = \epsilon^T + \epsilon^{sh} + \epsilon^{asr} \quad (39)$$

All concrete expansion-based models are based on the concept of free ASR expansion $\epsilon^{asr,free}$ (May, Wen, & Cope, 1992), i.e., the ASR-induced expansion that would have occurred for the same concrete under the same conditions but without stress. It is a scalar measure and corresponds with the uniaxially measured strain in stress-free conditions. The free ASR expansion creates the link between the reaction kinetics and the mechanics. Constitutive modelling of the free ASR expansion is discussed later. First, the modelling of the stress-dependency of the ASR expansion is discussed, i.e., the relationship between the free and the imposed expansion.

The simplest model assumes the imposed ASR expansion equal to the free ASR expansion in all directions, i.e., both stress independent and isotropic. In three dimensions, with six independent strain components (Voigt notation), its given by

$$\epsilon^{asr} = [1 \ 1 \ 1 \ 0 \ 0 \ 0]^T \epsilon^{asr,free} \quad (40)$$

This is considered as a thermal equivalent approach and is the current “engineering” practice in Norway (Johansen, 2022).

In more advanced formulations, the imposed expansion is stated on a rate form and is a function of the current stress state, given by

$$\dot{\epsilon}^{\text{asr}} = \mathbf{W}(\sigma) \dot{\epsilon}^{\text{asr,free}} \quad (41)$$

where the over-dot means differentiation with respect to time and \mathbf{W} is a vector-valued function of stress (σ) that accounts for reduction in the imposed ASR expansion in the compressed directions. As mentioned in the previous section, four different expansion behaviours have been experimentally observed. As a result, many formulations of the function \mathbf{W} exist in the literature.

A one-dimensional version (scalar valued function W) is shown in Figure 5-12. In this case, W expresses the fraction of the imposed to the free ASR expansion for uniaxially loaded concrete. The logarithmic function shown in the figure was proposed by (Charlwood, Solymar, & Curtis, 1992) and is widely used in material modelling. It ranges from 1, no reduction in expansion, for stresses greater than $-\sigma_L$, and to 0, no expansion, for stresses less than $-\sigma_u$. A linear or quadratic polynomial, or an exponential function for \mathbf{W} in range between σ_u and σ_L have been proposed by other researchers (Wen, 1993).

The material constants σ_L and σ_u depend on the concrete mix and should be determined from uniaxially restrained expansion experiments, see e.g. [Jones, Berra, Kongshaug]. Measured expansions under multiple sustained compressive stress levels are recommended to achieve a model for \mathbf{W} . The experimental investigation of (Berra, Faggiani, Mangialardi, & Paolini, 2010) found that the expansion under sustained compressive stress of 0.17 MPa was equal to the free expansion irrespective of concrete mix. The compressive stress σ_u necessary to stop the expansion ranges from 3 MPa to 10 MPa (Herrador, Martínez-Abella, & Rabuñal Dopico, 2008).

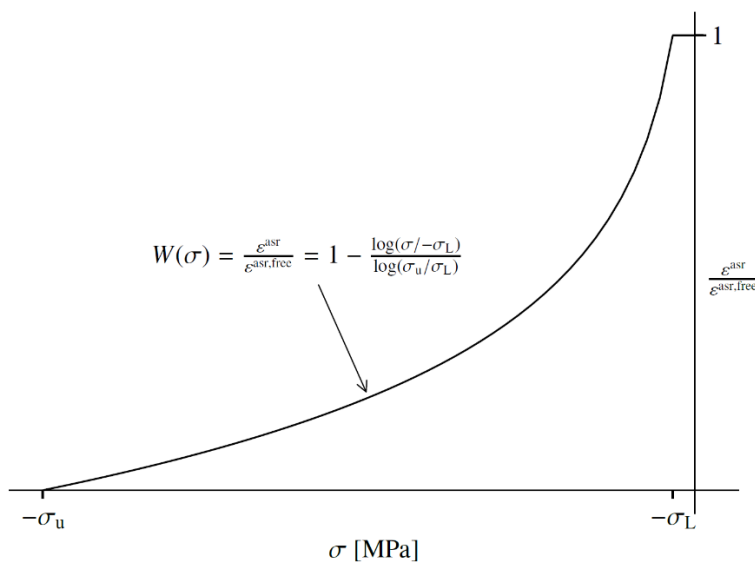


Figure 5-12: Stress-expansion relationship proposed by (Charlwood, Solymar, & Curtis, 1992); $W(\sigma)$ is the imposed expansion relative to the free expansion.

An extension of the one-dimensional model to three dimensions can be obtained by considering the expansion in the three principal stress directions independently (Charlwood, Solymar, & Curtis, 1992), given by:

$$\dot{\varepsilon}_i^{\text{asr}} = W(\sigma_i) \dot{\varepsilon}^{\text{asr,free}} \quad ; \quad i = 1, 2, 3 \quad (42)$$

This model suits the third expansion behavior mentioned in the previous section, i.e., when no or negligible expansion transfer occurs. On the other hand, if the volumetric expansion is expected to be conserved, the following model can be used (Jendele, Hájková, Šmilauer, & Červenka, 2018):

$$\dot{\varepsilon}_i^{\text{asr}} = \frac{3 W(\sigma_i)}{W(\sigma_1)+W(\sigma_2)+W(\sigma_3)} \dot{\varepsilon}^{\text{asr,free}} \quad ; \quad i = 1, 2, 3 \quad (43)$$

Other three-dimensional expansion models can be found in the literature (Saouma & Perotti, 2006) (Kawabata, Seignol, Martin, & Toutlemonde, 2016).

We have now seen how the stress-induced anisotropic expansion can be modeled. Nevertheless, we have not yet discussed the modelling of the evolution of ASR, and hence, the evolution of the free ASR expansion—the free ASR expansion is the link between the reaction kinetics and the mechanics. In the most sophisticated material models, the free ASR expansion relies on many fields such as temperature, moisture, and alkali content (Léger, Côté, & Tinawi, 1996) (Saouma & Perotti, 2006) (Pourbehi & van Zijl, 2019). In these advanced formulations, those fields are computed in the time domain for given boundary and initial conditions, and a unidirectional coupling with the mechanical problem is assumed, i.e., the temperature and the moisture affect the mechanics, but the mechanics is not affected by the temperature and moisture distribution within the structure.

The rate of free ASR expansion at a particular point in the structure is a function of temperature T and relative humidity RH . From a review of models that account for temperature and relative humidity, the free ASR expansion is often expressed on the following form:

$$\dot{\varepsilon}^{\text{asr,free}} = \zeta(t, T) g(RH) \dot{\varepsilon}_{\infty}^{\text{asr,free}} \quad (44)$$

In Eq. (44), $\zeta(t, T)$ is a chemical advancement function that ranges from 0 to 1 in time, i.e., from no reaction to final reaction. The s-shaped function proposed by (Larive, 1997) and (Ulm, Coussy, Kefei, & Larive, 2000), derived from chemo-poro-elastic considerations, is used among many researchers, e.g. (Saouma & Perotti, 2006) (Pourbehi & van Zijl, 2019). The function $g(RH)$ considers the influence of moisture/relative humidity on the expansion and ranges from 0 to 1, see (Léger, Côté, & Tinawi, 1996) (Saouma & Perotti, 2006). The constant $\dot{\varepsilon}_{\infty}^{\text{asr,free}}$ is the expansion potential of the concrete mix, the maximum expansion under sufficient water supply.

If the history of temperature and moisture can be computed for an existing structure, the free ASR expansion field in the spatial coordinates (x, y, z) and time (t) can be computed in advance of mechanical problem.

5.5.3 Modelling material degradation

In addition to expansion, ASR leads to a reduction in stiffness and strength. Figure 5-13 shows the reduction in modulus of elasticity and tensile strength with respect to ASR expansion (Kongshaug S. S.,

Load effects of alkali-silica reaction in reinforced concrete beam bridges - Material testing, Constitutive modelling and Numerical simulation); the results are adapted from the experimental works of (Smaoui, Bissonnette, Bérubé, Fournier, & Durand, 2005) and (Kongshaug S. , et al., 2020). In the same figure, a model functions for the reduction in modulus of elasticity is approximated to the experimental results. This one-dimensional model was first proposed by (Wen, 1993), and in (Kongshaug, Hendriks, Kanstad, & Markeset, 2022) it was generalized to three dimensions, expressed in terms of a compliance relation.

The same one-dimensional model function, see Figure 5-13, suits the reduction in tensile strength. In (Kongshaug, Hendriks, Kanstad, & Markeset, 2022), the reduction in tensile strength was combined with a smeared crack formulation. However, an isotropic reduction was assumed, despite the anisotropic degradation experimentally observed for ASR-affected concrete.

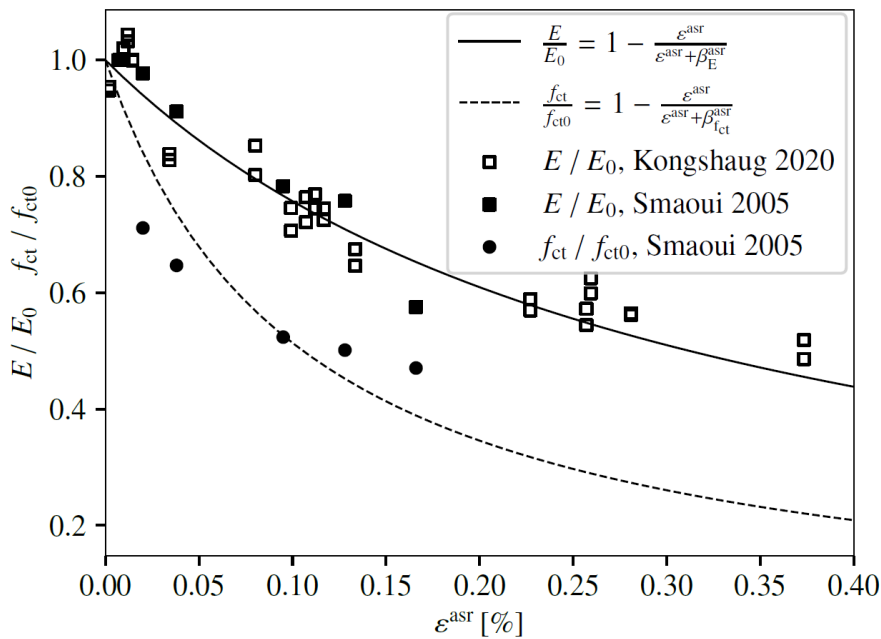


Figure 5-13: Evolution in modulus of elasticity and direct tensile (relative to initial/undamaged value) strength for increasing ASR expansions (Kongshaug S. S., Load effects of alkali-silica reaction in reinforced concrete beam bridges - Material testing, Constitutive modelling and Numerical simulation).

5.5.4 Modelling reinforced concrete structures affected by ASR—important aspects and challenges.

It is only the concrete that expands due to ASR, so to capture the internal restraint effect owing to expansion incompatibility between concrete and reinforcement, rebars must be part of the structural model. However, an engineering approach that accounts for the reinforcement on the expansion but where the reinforcement is not part of the structural analysis is suggested in (Johansen, 2022) (Stemland, Johansen, & Kanstad, Load Effects of ASR-induced Expansion in Reinforced Concrete and Their Consequences for Structural Assessment, 2023). It should be noted that this method is akin to a drying shrinkage consideration (with opposite sign), where the stress-dependency of the ASR expansion is neglected. Experimental evidence shows that the stress-dependency of the ASR-expansion is strong and non-linear, and therefore, should be included. The consequence of simplifications is investigated in (Kongshaug, Larssen, Hendriks, Kanstad, & Markeset, 2021). In summary, an accurate structural analysis of ASR-affected RC structures requires the inclusion of reinforcement bars.

Different ASR-affected concrete mixes behave differently, and as a result, many material models exist. The choice of expansion model should be determined based on experimental studies for the modelled concrete. Labelling the concrete to one of the four expansion categories detailed in Section 5.5.1 is helpful in selecting a suitable expansion model. The shape of stress-expansion relationships, and the compressive stress at which the expansion ceases are very influential on the results of the structural analysis (Kongshaug, Larssen, Hendriks, Kanstad, & Markeset, 2021).

As discussed by (Kongshaug S. S., Load effects of alkali-silica reaction in reinforced concrete beam bridges - Material testing, Constitutive modelling and Numerical simulation), a common challenge for the application of material models, is the determination of the input fields to the structural analysis. If, for instance, the material model relies on the input of moisture and temperature, these fields—in space and time—must be determined before the structural analysis. This requires solving the corresponding transient problem, and hence, the initial and boundary conditions must be known for the structure’s history. These are hardly available for an existing structure. Besides, these models are complex and difficult to implement. Indeed, there seems to be a trend in adding complexity to the material model without questioning their relative importance in estimating the structural response.

(Kongshaug, Hendriks, Kanstad, & Markeset, 2022) developed a structural analysis method for existing structures when dealing with unknown input fields. Its use was demonstrated on Elgeseter Bridge in Norway. The approach is based on solving an inverse problem. Only one input field was assumed—the free ASR expansion $\varepsilon^{asr,free}$. The free ASR expansion is considered as an unknown and is back-calculated (calibrated) from a set of displacement measurements. The calculated cracks are used to validate the solution.

5.6 Safety format

Eurocode 2 (FprEN-1992-1-1) recommends safe design of concrete structures based on partial factor method (PFM) applied to the limit state design. The PFM is a semi-probabilistic method, where safety format is applied to the explicitly categorized and standardized uncertainties (e.g., material properties), failure modes (e.g., design cases), and failure consequences (e.g., consequence classes) and calibrated within those frames (Baravalle & Kohler, 2016). Because of those explicit frames, such safety format is easy to use and reproducible by structural engineers. However, design optimisation freedom and non-typical approaches like use of novel materials, innovative methods, and techniques not defined within the standards are naturally compromised. The calibration of semi-probabilistic approaches is based on the probabilistic codes and reliability methods (JCSS, 2001), which are used continuously to update and extend the optimal application of the former one. One such update is consideration of the adjusted material factors if the structural non-linear analysis is applied (Annex A), where new values are specified as shown in the Table 5-2 together with standard material partial factors.

Table 5-2: EC2 modification of partial material factors when using non-linear FEA.

Partial material factor	Persistent and transient design situation			Accidental design situation		
	γ_s	γ_c	γ_v	γ_s	γ_c	γ_v
Table 4.3, EC2	1.25	1.5	1.4	1.00	1.15	1.15
Annex A: Non-linear analysis + model uncertainty	1.2	1.46	1.31	1.09	1.16	1.16

Modified partial material factors can be applied when model uncertainty (γ_{Rd}) is considered separately:

$$R_d = \frac{R\{X_d; a_d\}}{\gamma_{Rd}} \quad (45)$$

Here, R is resistance based on non-linear analysis and X_d is based on partial material factors from Annex A.

Safety format for non-linear analysis of reinforced concrete structures is an ongoing research effort (Yu, Ruiz, & Muttoni, 2022). The current safety format, i.e., partial safety factor format, present in codes consider two failure modes, i.e., compressive strength of concrete and tensile strength of steel, calibrated independently without the interaction effects considered. The ongoing research into including multiple different failure modes as ultimate limit state has resulted in the proposal of Global Safety Factor Format and method to evaluate the possibility of multimode failure (bending, shear, cracking, fatigue) and additional safety factor.

Schlune (Schlune, Plos, & Gylltoft, 2012) method was included within fib Model Code 2010 as a one resistance factor approach. It proposes including mean material properties ($f_{cm, is}$ - mean in situ compressing strength, f_{ym} - mean yield strength of steel) and nominal geometrical data a_{nom} in the non-linear models and a single resistance factor γ_R to ensure the targeted reliability.

$$R_d = \frac{R(f_{cm, is}, f_{ym}, a_{nom})}{\gamma_R}, \quad \gamma_R = \frac{\exp(\alpha_R \beta V_R)}{\theta_m}, \quad V_R = \sqrt{V_g^2 + V_m^2 + V_f^2} \quad (46)$$

Here, the log-normal probability distribution of material parameters is assumed, and uncertainties connected to the modelling approach are summarized within the mean ratio of the experimental and predicted resistance $\theta_m \in (0.7, 1.2)$, while coefficient of variation for geometry, material and model are calculated as a root mean square value V_R . Since coefficient of variation for material is now a single value V_f , the formula for its evaluation requires information on the variations of both steel and concrete properties as well as results from non-linear analysis for lowest value of steel resistance and lowest value of concrete resistance respectively. Some numerical examples of variations are shown in Table 5-3.

Table 5-3: European Concrete Platform (2008) –coefficient of variations.

Uncertainty type	Coefficient of Variations	
	Steel	Concrete
Model	$V_{\theta,R} = 2.5\%$	$V_{\theta,R} = 5\%$
Geometry	$V_g = 5\%$	$V_g = 5\%$
Material	$V_f = 4\%$	$V_f = 15\%$

6 Conclusion

This document reports the state-of-the-art for performing NLFEA to assess the structural integrity of deteriorated RC structures. Numerous approaches for modelling the composite behaviour of concrete and reinforcing and prestressing steel were addressed. No specific recommendations for choice of material models were provided this time around, as this will be covered at a later stage in the project. Instead, it was emphasized that the chosen composition of material models needs be consistent with one another. Furthermore, it was shown that deterioration effects caused by corrosion of reinforcing steel can be accounted for by modifying the undamaged stress-strain curve of the naked steel or the tension chord model. References on how to modify the behaviour were provided. Moreover, modelling deterioration effects caused by ASR was also addressed. It was argued that this could be accounted for by separating the mechanical strains from the total strains by using a proper expansion model for the ASR strains. Finally, a proper safety format to assess the structural integrity of deteriorated RC structures when applying NLFEA was addressed. It was found that both partial safety factor and global safety factor methods could be applied for this purpose.

7 Future research

The findings in this STAR serves as legitimate point of departure for the project. Hence, future research tasks will more specifically address

- Proper composition of material models.
- How the stress-strain curves of both naked steel and tension chord models should be modified due to deterioration caused by corrosion.
- How ASR strains can be derived with proper expansion models to separate the mechanical strains from the total strains.
- Choice of proper safety format.



8 References

- Abdel-Jaber, M., & El-Nimri, R. (2022). Comparative investigation, numerical modeling, and buckling analysis of one-way reinforced concrete wall panels. *Results in Engineering*, 100-459.
- Abra, O., & Ftima, M. B. (2020). Development of a new design approach of reinforced concrete structures based on strength reduction method. *Engineering Structures*, 110192.
- Ahmed, T., Burley, E., Rigden, S., & Abu-Tair, A. (2003). The effect of alkali reactivity on the mechanical properties of concrete. *Construction Building Materials*.
- Ahmed, T., M.A, Burley, E., & Rigden, S. (1999). The effect of alkali—silica reaction on the fatigue behaviour of plain concrete tested in compression, indirect tension and flexure. *Magazine of Concrete Research*.
- Alabduljabbar, H., Haido, J. H., Alyousef, R., Yousif, S. T., McConnell, J., Wakil, K., & Jermsittiparsert, K. (2020). Prediction of the flexural behavior of corroded concrete beams using combined method. *Structures*, 1000-1008.
- Alami, E. E., Fekak, F.-E., Garibaldi, L., & Elkhalfi, A. (2021). A numerical study of pitting corrosion in reinforced concrete structures. *Journal of Building Engineering*, 102789.
- Alanazi, N., & Susmel, L. (2022). Theory of Critical Distances and static/dynamic fracture behaviour of un-reinforced concrete: length scale parameters vs. material meso-structural features. *Engineering Fracture Mechanics*, 108220.
- Alfaiate, J., & Sluys, L. (2023). A novel, total-iterative approach to model quasi-brittle materials. *Engineering Fracture Mechanics*, 108955.
- Alhanaee, S., Yi, Y., & Schiffer, A. (2018). Ultimate pressure capacity of nuclear reactor containment buildings under unaged and aged conditions. *Nuclear Engineering and Design*, 128-139.
- Al-kroom, H., Reimer, A., Alghrir, Y., Thneibat, M., & Schmid, V. (2021). Experimental and numerical investigation on the saw-tooth connector subjected to compressive load. *Journal of Constructional Steel Research*, 106485.
- Allam, S. M., Elbakry, H. M., & Arab, I. S. (2018). Exterior reinforced concrete beam column joint subjected to monotonic loading. *Alexandria Engineering Journal*, 4133-4144.
- Allard, A., Bilodeau, S., Pissot, F., Fournier, B., Bastien, J., & Bissonnette, B. (2018). Expansive behaviour of thick concrete slabs affected by alkali-silica reaction (ASR). *Construction Building Materials*.
- Aryan, H., & Gentruck, B. (2021). Influence of alkali-silica reaction on the shear capacity of reinforced concrete beams with minimum transverse reinforcement. *Engineering Structures*.
- Bach, F., Thorsen, T. S., & Nielsen, M. P. (1993). Load-carrying capacity of structural members subjected to alkali-silica reactions. *Construction Building Materials*.
- Bagge, N., Popescu, C., & Elfren, L. (2017). Failure test on concrete bridges: Have we learnt the lesson?
- Bao, Y., Feng, D., Ma, N., Zhu, H., & Rabczuk, T. (2018). Experimental and numerical study on structural performance of reinforced concrete box sewer with localized extreme defect. *Underground Space*, 166-179.
- Baravalle, M., & Kohler, J. (2016). Risk and Reliability Based Calibration of Design Codes for. *2nd International Symposium on Submerged Floating Tunnels and Underwater Tunnel Structures*, 247-254.
- Barbosa, R. A., Hansen, S. G., Hansen, K. K., Hoang, L. C., & Grelk, B. (2018). Influence of alkali-silica reaction and crack orientation on the uniaxial compressive strength of concrete cores from slab bridges. *Construction Building Materials*.
- Basha, A., Tayeh, B. A., Maglad, A. M., & Mansour, W. (2023). Feasibility of improving shear performance of RC pile caps using various internal reinforcement configurations: Tests and finite element modelling. *Engineering Structures*, 116340.
- Benakli, S., Bouafia, Y., Oudjene, M., Boissière, R., & Khelil, A. (2018). A simplified and fast computational finite element model for the nonlinear load-displacement behaviour of reinforced concrete structures. *Composite Structures*, 468-477.

- Berra, M., Faggiani, G., Mangialardi, T., & Paolini, A. E. (2010). Influence of stress restraint on the expansive behaviour of concrete affected by alkali-silica reaction. *Cement and Concrete Research*.
- Bilodeau, S. B., Allard, A., Bastien, J. E., Pissot, F. O., Fournier, B. T., & Mitchell, D. (2016). Performance Evaluation of Thick Concrete Slabs Affected by Alkali-Silica Reaction (ASR) Part II: Structural Aspects. *15th ICAAR*. Brazil.
- Borbon-Almada, N. S.-M. (2019). Peridynamic modelling of reinforced concrete structures. *Engineering Failure Analysis*, 266-274.
- Borst, d. R., & Nauta, P. (1985). Non-orthogonal cracks in a smeared finite element model. *Engineering Computations*, 35-46.
- Brugel, K. (2001). *Modelling of strength development in hardening concrete*. IPACS Report, Luleå University of Technology, ISBN:91-89580-40-0.
- Cairns, J., Plizzari, G., Du, Y., Law, D., & Franzoni, C. (2005). Mechanical properties of corrosion-damaged reinforcement. *ACI Materials Journal*, 102(4).
- Carvalho, J. G., Sousa, C., Granja, J., Faria, R., Schlicke, D., & Azenha, M. (2020). 3D numerical simulation of the cracking behaviour of a RC one-way slab under the combined effect of thermal, shrinkage and external loads. *Engineering Structures*, 110493.
- Castaldo, P., Gino, D., & Mancini, G. (2019). Safety formats for non-linear finite element analysis of reinforced concrete structures: discussion, comparison and proposals. *Engineering Structures*, 136-153.
- Castaldo, P., Gino, D., Bertagnoli, G., & Mancini, G. (2018). Partial safety factor for resistance model uncertainties in 2D non-linear finite element analysis of reinforced concrete structures. *Engineering Structures*, 746-762.
- CEN. (2004). *Eurocode 2: Design of concrete structures - Part 1-1: General rules and rules for buildings*. European Committee for Standardization.
- Červenka, J., & Papanikolaou, V. K. (2008). Three dimensional combined fracture–plastic material model for concrete. *International Journal of Plasticity*, 2192-2220.
- Cervenka, V., Rimkus, A., Gribniak, V., & Cervenka, J. (2022). Simulation of the crack width in reinforced concrete beams based on concrete fracture. *Theoretical and Applied Fracture Mechanics*, 121. doi:<https://doi.org/10.1016/j.tafmec.2022.103428>
- Cervera, M., Tesei, C., & Ventura, G. (2018). Cracking of quasi-brittle structures under monotonic and cyclic loadings: A d+/d– damage model with stiffness recovery in shear. *International Journal of Solids and Structures*, 148-171.
- Chana, P. S., & Korobokis, G. A. (1991). Structural performance of reinforced concrete affected by alkali silica reaction.
- Chang, T., Lee, C.-L., Carr, A., & Dhakal, R. (2019). Numerical evaluations of a novel membrane element in simulations of reinforced concrete shear walls. *Engineering Structures*, 109592.
- Charlwood, R., Solymar, S., & Curtis, D. (1992). A review of alkali aggregate reactions in hydroelectric plants and dams. *The international conference of alkali-aggregate reactions in hydroelectric plants and dams*.
- Chen, A. C., & Chen, W. (1975). Constitutive Relations for Concrete. *Journal of the Engineering Mechanics Division*, 465-481.
- Chen, J.-Y., Li, W., Han, L.-H., Wang, F.-C., & Mu, T.-M. (2019). Structural behaviour of concrete-encased CFST box stub columns under axial compression. *Journal of Constructional Steel Research*, 248-262.
- Chen, Z., Li, X., Yang, Y., Zhao, S., & Fu, Z. (2018). Experimental and numerical investigation of the effect of temperature patterns on behavior of large scale silo. *Engineering Failure Analysis*, 543-553.
- Chrisp, T. M., Waldron, P., & Wood, J. G. (1993). Development of a non-destructive test to quantify damage in deteriorated concrete. *Magazine of Concrete Research*.

- Comi, C., Kirchmayr, B., & Pignatelli, R. (2011). Two-phase damage modeling of concrete affected by alkali-silica reaction under variable temperature and humidity conditions. *International Journal of Solids and Structures*.
- Cosmin Popescu, T. D. (2023). *DT methods and sensors for existing concrete structures*. SINTEF.
- Courtier, R. (1990). The assessment of ASR-affected structures. *Cement and Concrete composites*.
- D., D.-d.-C., V., C., & R., G.-e.-C. (2018). Model uncertainty in discrete and smeared crack prediction in RC beams under flexural loads. *Engineering Fracture Mechanics*, 532-543.
- den Uijil, J., & Kaptijn, N. (2002). Structural Consequences of ASR: An Example of Shear Capacity. *Heron*.
- Dey, S., & Karthik, M. M. (2019). Modelling four-pile cap behaviour using three-dimensional compatibility strut-and-tie method. *Engineering Structures*, 109499.
- Dias-da-Costa, D., Cervenka, V., & Graça-e-Costa, R. (2018). Model uncertainty in discrete and smeared crack prediction in RC beams under flexural loads. *Engineering Fracture Mechanics*, 532-543.
- Dobry, J., Wolfger, H., & Benko, V. (2022). Reliability of slender concrete columns designed according to the Eurocodes. *Engineering Structures*, 114266.
- Dr. Ing. A. Aas-Jakobsen AS. (2013). *Elgeseter bridge—Report from special survey in 2012*.
- Du, Y., Clark, L., & Chan, A. (2005). Residual capacity of corroded reinforcing bars. *Magazine of Concrete Research*, 57(3), 135-147. doi:<https://doi.org/10.1680/macr.2005.57.3.135>
- Dunant, C., & Scrivener, K. (2012). Effects of uniaxial stress on alkali-silica reaction induced expansion of concrete. *Cement and Concrete Research*.
- El-Joukhadar, N., Dameh, F., & Pantazopoulou, S. (2023). Seismic Modelling of Corroded Reinforced Concrete Columns. *Engineering Structures*, 115251.
- Esposito, R., & Hendriks, M. (2019). Literature review of modelling approaches for ASR in concrete: a new perspective. *European Journal of Environmental and Civil Engineering*.
- Esposito, R., Anac, C., Hendriks, M., & Copuroglu, O. (2016). Influence of the Alkali-Silica Reaction on the Mechanical Degradation of Concrete. *Journal of Materials in Civil Engineering*.
- Faron, A., & Rombach, G. A. (2020). Simulation of crack growth in reinforced concrete beams using extended finite element method. *Engineering Failure Analysis*, 104-698.
- Faron, A., & Rombach, G. A. (2020). Simulation of crack growth in reinforced concrete beams using extended finite element method. *Engineering Failure Analysis*, 104698.
- Fei, W., Yang, Z. J., & Sun, T. (2019). Ground freezing impact on laterally loaded pile foundations considering strain rate effect. *Cold Regions Science and Technology*, 53-63.
- Freiesleben Hansen, P. a. (1977). *Maturity computer for controlled curing and hardening of concrete (in Danish: Måleinstrument til kontrol af betons hærkning)*. Nordisk Betong 1 (1977) 21-25.
- Gautam, B., Penesar, D., Sheikh, S., & Vecchio, F. (2017). Effect of Multiaxial Stresses on Alkali-Silica Reaction Damage of Concrete. *ACI Materials Journal*.
- Giaccio, G., Torrijos, M., Tobes, J., Batic, O., & Zerbino, R. (2009). Development of alkali-silica reaction under compressive loading and its effects on concrete behavior. *ACI Materials Journal*.
- Giaccio, G., Zerbino, R., Ponce, J. M., & Batic, O. R. (2008). Mechanical behaviour of concretes damaged by alkali-silica reaction. *Cement and Concrete Research*.
- Giaccio, G., Zerbino, R., Ponce, J., & Batic, O. (2008). Mechanical behavior of concretes damaged by alkali-silica reaction. *Cement and Concrete Research*.
- Goh, C. Y., & Hrynyk, T. D. (2020). Nonlinear finite element analysis of reinforced concrete flat plate punching using a thick-shell modelling approach. *Engineering Structures*, 111250.
- Gomes, J., Carvalho, R., Sousa, C., Granja, J., Faria, R., Schlicke, D., & Azenha, M. (2020). 3D numerical simulation of the cracking behaviour of a RC one-way slab under the combined effect of thermal, shrinkage and external loads. *Engineering Structures*, 110493.
- Gravel, C., Ballivy, G., Khayat, K., Quirion, M., & Lachemi, M. (2000). Expansion of AAR concrete under triaxial stresses: Simulation with instrumented concrete block. *11th International Conference on Alkali-Aggregate Reaction*. Quebec, Canada.

- Guner, S. (2023). Analysis methodology and design verification for strengthening moment-resisting caisson foundations. *Engineering Structures*, 115582.
- Guo, H., Dong, Y., Bastidas-Arteaga, E., & Gu, X.-L. (2021). Probabilistic failure analysis, performance assessment, and sensitivity analysis of corroded reinforced concrete structures. *Engineering Failure Analysis*, 105328.
- Haefliger, S. (2022). *Load-deformation behaviour of reinforced concrete structures affected by local corrosion* (Vol. PhD Thesis). Zürich: ETH Zürich.
- Hafiz, A., Schumacher, T., & Raad, A. (2022). A self-referencing non-destructive test method to detect damage in reinforced concrete bridge decks using nonlinear vibration response characteristics. *Construction and Building Materials*, 125924.
- Hájková, K., Šmilauer, V., Jendele, L., & Červenka, J. (2018). Prediction of reinforcement corrosion due to chloride ingress and its effects on serviceability. *Engineering Structures*, 768-777.
- Hanif, M., Ibrahim, Z., Ghaedi, K., H., H., & Javanmardi, A. (2018). Damage assessment of reinforced concrete structures using a model-based nonlinear approach – A comprehensive review. *Construction and Building Materials*, 846-865.
- Hansen, S. G., & Hoang, L. (2019). Influence of Alkali-Silica Reaction on the Shear Capacity of Reinforced Concrete Slabs Without Shear Reinforcement.
- Hansen, S. G., Barbosa, R., Cao, L., & Hansen, K. (2016). Shear capacity of ASR damaged structures-in-depth analysis of some in-situ shear tests on bridge slabs.
- Hasan, M., Qasem, M., Muhamad, R., & Mutafi, A. (2022). 3D finite element modeling of precast wall panels connection under monotonic loading. *Materials Today: Proceedings*, 943-953.
- Hasan, M., R., M., Q., & Muhamad. (2023). Finite element modeling of precast reinforced concrete wall with dual boundary elements under lateral load. *Materials Today: Proceedings*, 2214-7853.
- He, Y., & Fan, W. (2023). Improved plastic-damage cap model for shear behavior predictions of plain and reinforced concrete members. *Engineering Structures*, 116070.
- Hendriks, M., de Boer, A., & Belletti, B. (2016). *Guidelines for Nonlinear Finite Element Analysis of Concrete Structures*. Netherlands: Rijkswaterstaat Ministry of Infrastructure and the Environment.
- Hernández-Díaz, A. M., Pérez-Aracil, J., Casillas-Perez, D., Pereira, E., & Salcedo-Sanz, S. (2022). Hybridizing machine learning with metaheuristics for preventing convergence failures in mechanical models based on compression field theories. *Applied Soft Computing*, 109654.
- Herrador, M., Martínez-Abella, F., & Rabuñal Dopico, J. (2008). Experimental evaluation of expansive behavior of an old-aged ASR-affected dam concrete: methodology and application. *Materials and Structures*.
- Hillerborg, A., Modéer, M., & Petersson, P.-E. (1976). Analysis of crack formation and crack growth in concrete by means of fracture mechanics and finite elements. *Cement and Concrete Research*, 773-781.
- Institution of Structural Engineers. (1992). *Structural Effects of Alkali-Silica Reaction: Technical Guidance on the Appraisal of Existing Structures*.
- International Federation for Structural Concrete (fib—Fédération Internationale du Béton)*. (2010). Berlin, Germany: Fib Model Code for Concrete Structures 2010; Ernst & Sohn:
- Jang, S. Y. (2011). *Seung Yuo Jang et al. Effect of crack width on chloride diffusion coefficients of concrete by steady-state migration tests*. Cement and Concrete Research.
- JCSS. (2001). *The JCSS Probabilistic Model Code, in Part 1 - Basis of Design*.
- Jendele, L., Hájková, K., Šmilauer, V., & Červenka, J. (2018). Modeling alkali-silica-reaction in reinforced concrete structures combining kinetics and fracture mechanics.
- Jensen, V. (2004). Alkali-silica reaction damage to Elgeseter Bridge, Trondheim, Norway: a review of construction, research and repair up to 2003. *Materials characterization*.
- Jin, L., Wang, Z., Zhang, R., & Du, X. (2021). Mesoscopic simulation on flexural behavior of single-way reinforced concrete slab with rebars subjected to localized corrosion. *Structures*, 815-827.

- Jingfeng, W., Ziming, H., Shen, Q., Guoqiang, L., & Zhenghu, H. (2023). Mechanical investigation and design of axially-loaded concrete columns reinforced with grade 700MPa reinforcing bars. *Structures*, 1148-1166.
- Johansen, H. (2022). *Bæreevneklassifisering av bruer med alkalireaksjoner, Svv Rapport Nr. 855*.
- Jones, A. E., & Clark, L. A. (1998). The effects of ASR on the properties of concrete and the implications for assessment. *Engineering Structures*.
- Jones, A., & Clark, L. (1996). The effects of restraint on ASR expansion of reinforced concrete. *Magazine of Concrete Research*.
- Ju, J. (1989). On energy-based coupled elastoplastic damage theories: Constitutive modeling and computational aspects. *International Journal of Solids and Structures*, 803-833.
- Kagimoto, H., Yasuda, Y., & Kawamura, M. (2014). ASR expansion, expansive pressure and cracking in concrete prisms under various degrees of restraint. *Cement and Concrete Research*.
- Kanstad, T. T. (2002). *Mechanical properties of young concrete: Part II: Determination of model parameters and test program proposals*. *Materials and Structures* 36 (2002) 226-230.
- Kaufmann, W., & Marti, P. (1998). Structural Concrete: Cracked Membrane Model. *Journal of Structural Engineering*, 124(12).
- Kawabata, Y., Seignol, J. F., Martin, R. P., & Toutlemonde, F. (2016). Influence of creep and stress states on alkali-silica reaction induced-expansion of concrete under restraint. *15th Int. Conf. Alkali-Aggregate Reaction in Concrete*.
- Kawamura, M., & Iwahori, K. (2004). ASR gel composition and expansive pressure in mortars under restraints. *Cement and Concrete Composites*.
- Kongshaug, S. S. (n.d.). Load effects of alkali-silica reaction in reinforced concrete beam bridges - Material testing, Constitutive modelling and Numerical simulation. *PhD Thesis*.
- Kongshaug, S. S., Larssen, R. M., Hendriks, M. A., Kanstad, T., & Markeset, G. (2021). Load effects in reinforced concrete beam bridges affected by alkali-silica reaction—Constitutive modelling including expansion, cracking, creep and crushing. *Engineering structures*.
- Kongshaug, S. S., Oseland, O. W., Kanstad, T., Hendriks, M., Rodum, E., & Markeset, G. (2020). Experimental investigation of ASR-affected concrete - The influence of uniaxial loading on the evolution of mechanical properties, expansion and damage indices. *Construction and Building Materials*.
- Kongshaug, S., Hendriks, M., Kanstad, T., & Markeset, G. (2022). Toward identifying the ASR-induced stresses from displacement measurements and crack observations—Demonstration on a beam bridge in Norway. *Engineering Structures*.
- Kongshaug, S., Oseland, O., Kanstad, T., Hendriks, M., Rodum, E., & Markeset, G. (2020). Experimental investigation of ASR-affected concrete—The influence of uniaxial loading on the evolution of mechanical properties, expansion and damage indices. *Construction and Building Materials*.
- Kueres, S., & Hegger, J. (2020). Variable strut inclination model for shear design of FRP reinforced concrete members with shear reinforcement. *Engineering Structures*, 110154.
- Kurumatani, M., Soma, Y., & Terada, K. (2019). Simulations of cohesive fracture behavior of reinforced concrete by a fracture-mechanics-based damage model. *Engineering Fracture Mechanics*, 392-407.
- Larive, C. (1997). *Apports combinés de l'expérimentation et de la modélisation à la compréhension de l'alkali-réaction et de ses effets mécaniques*. Ecole nationale des ponts et chaussées.
- Lee, J., & Fenves, L. (1998). Plastic-Damage Model for Cyclic Loading of Concrete Structures. *Journal of Engineering Mechanics*, 892-900.
- Lee, S.-H., Abolmaali, A., Shin, K.-J., & Lee, H.-D. (2020). ABAQUS modeling for post-tensioned reinforced concrete beams. *Journal of Building Engineering*, 101273.
- Leemann, A., G'ora, M., Lothenbach, B., & Heuberger, M. (2024). Alkali silica reaction in concrete - Revealing the expansion mechanism by surface force measurements. *Cement and Concrete Research*.

- Léger, P., Côté, P., & Tinawi, R. (1996). Finite element analysis of concrete swelling due to alkali-aggregate reactions in dams. *Computers & structures*.
- Li, Z., Guo, J., Jin, S., Zhang, P., & Gong, J. (2022). Fragility analysis and probabilistic safety evaluation of the nuclear containment structure under different prestressing loss conditions. *Annals of Nuclear Energy*, 108862.
- Liaudat, J., Carol, I., López, C., & Saouma, V. (2018). ASR expansions in concrete under triaxial confinement. *Cement and Concrete Composites*.
- Lindgård, J. (2013). *Alkali-silica-reaction (ASR) - Performance testing*. NTNU.
- Liu, Q., & Su, R. K. (2018). A displacement-based inverse analysis method to estimate in-situ Young's modulus of steel rust in reinforced concrete. *Engineering Fracture Mechanics*, 114-128.
- Lublinter, J., Oliver, J., Oller, S., & E. Oñate. (1989). A plastic-damage model for concrete. *International Journal of Solids and Structures*, 299-326.
- Marti, P., Alvarez, M., Kaufmann, W., & Sigrist, V. (1998). Tension Chord Model for Structural Concrete. *Structural Engineering International*.
- Marzec, I., Tejchman, J., & Mróz, Z. (2019). Numerical analysis of size effect in RC beams scaled along height or length using elasto-plastic-damage model enhanced by non-local softening. *Finite Elements in Analysis and Design*, 1-20.
- Mata-Falcón, J., Tran, D., Kaufmann, W., & Navrátil, J. (2018). Computer-aided stress field analysis of discontinuity concrete regions. *Computational Modelling of Concrete Structures*. Meschke, Pichler & Rots.
- May, I., Wen, H. X., & Cope, R. (1992). The modelling of the effects of AAR expansion on reinforced concrete members. *The Ninth International Conference on Alkali-Aggregate Reaction in Concrete*.
- Mazars, J. (1986). A description of micro- and macroscale damage of concrete structures. *Engineering Fracture Mechanics*, 729-737.
- Multon, S., & Toutlemonde, F. (2006). Effect of applied stresses on alkali-silica reaction-induced expansion. *Cement and Concrete Research*.
- Multon, S., Seignol, J., & Toutlemonde, F. (2005). Structural behavior of concrete beams affected by alkali-silica reaction. *ACI Materials Journal*.
- Multon, S., Seignol, J., & Toutlemonde, F. (2006). Chemomechanical assessment of beams damaged by alkali-silica reaction. *Journal of materials in civil engineering*.
- N. Scattarreggia, A. O. (2023). Failure analysis of ageing RC bridges: The cases of the Polcevera viaduct and the Caprigliola bridge. *Life-Cycle of Structures and Infrastructure Systems*.
- Nascimbene, R., & Bianco, L. (2021). Cyclic response of column to foundation connections of reinforced concrete precast structures: Numerical and experimental comparisons. *Engineering Structures*, 113214.
- Nasiri, E., & Liu, Y. (2019). The out-of-plane behaviour of concrete masonry infills bounded by reinforced concrete frames. *Engineering Structures*, 406-420.
- Noël, M., Sanchez, L., & Tawil, D. (2017). Structural Implications of Internal Swelling Reactions in Concrete: Review & Research Needs. *Magazine of Concrete Research*.
- NS-EN1992. (n.d.). *NS EN 1992-2:2005 rules, Design of concrete Structures - Concrete bridges - Design and detailing*. Standards Norway.
- NS-EN206. (n.d.). *NS-EN 206:2013+NA:2014: NS-EN Concrete - Specification, performance, production and conformity*. Oslo: Standards Norway.
- Ortiz, M. (1985). A constitutive theory for the inelastic behavior of concrete. *Mechanics of Materials*, 67-93.
- Osmolska, J., Kanstad, T., A.N., H. M., & G, M. (2022). Numerical investigation into the effects of corrosion on the shear performance of pretensioned bridge girders with cast-in-place slabs. *Structures*, 1447-1468.



- Osmolska, M., Kanstad, T., Hendriks, M., & Markeset, G. (2022). Numerical investigation into the effects of corrosion on the shear performance of pretensioned bridge girders with cast-in-place slabs. *Structures*, 1447-1468. doi:<https://doi.org/10.1016/j.istruc.2022.10.129>
- Panahi, H., & Genikomsou, A. S. (2022). Comparative evaluation of concrete constitutive models in non-linear finite element simulations of slabs with different flexural reinforcement ratios. *Engineering Structures*, 113617.
- Paz, G. L., Marques, M. G., & Ruas, S. R. (2022). Numerical analysis of reinforced concrete columns strengthened with sleeve wedge bolts and a self compacting concrete layer. *Structures*, 726-737.
- Peng, R.-X., & Qiu, W.-L. (2021). Research on freeze-thaw damage to RC column based on incompatibility deformation from pores. *Engineering Structures*, 112462.
- Peng, R.-x., Qiu, W.-l., & Jiang, M. (2022). Frost resistance performance assessment of concrete structures under multi-factor coupling in cold offshore environment. *Building and Environment*, 109733.
- Pourbehi, M. S., & van Zijl, G. P. (2019). Seismic analysis of the kleinplaas dam affected by alkali-silica reaction using a chemo-thermo-mechanical finite element numerical model considering fluid structure interaction. *Journal of Advanced Concrete Technology*.
- Qasem, M., Hasan, M., Muhamad, R., & Mutafi, A. (2022). Non-linear 3D finite element analysis of precast reinforced concrete Beam-Column joint under monotonic static load. *Materials Today: Proceedings*, 746-757.
- Rad, M. M., Ibrahim, S. K., & Lógó, J. (2022). Limit design of reinforced concrete haunched beams by the control of the residual plastic deformation. *Structures*, 987-996.
- Rad, M., Ibrahim, S. K., & Lógó, J. (2022). Limit design of reinforced concrete haunched beams by the control of the residual plastic deformation. *Structures*, 987-996.
- Resende, L. (1987). A Damage mechanics constitutive theory for the inelastic behaviour of concrete. *Computer Methods in Applied Mechanics and Engineering*, 57-93.
- Rombach, G., & Faron, A. (2019). Numerical analysis of shear crack propagation in a concrete beam without transverse reinforcement. *Procedia Structural Integrity*, 766-773.
- Rots, J. G., & Blaauwendraad, J. (1989). Crack models for concrete, discrete or smeared? Fixed, multi-directional or rotating? *HERON*.
- Russo, G., & Romano, F. (1992). Cracking Response of RC Members Subjected to Uniaxial Tension. *Journal of Structural Engineering*.
- Sanchez, L. F., Fournier, B., Jolin, M., & Bastien, J. (2014). Evaluation of the Stiffness Damage Test (SDT) as a tool for assessing damage in concrete due to ASR: Test loading and output responses for concretes incorporating fine or coarse reactive aggregates. *Cement and Concrete Research*.
- Sanchez, L. F., Fournier, B., Jolin, M., Mitchell, D., & Bastien, J. (2017). Overall assessment of Alkali-Aggregate Reaction (AAR) in concretes presenting different strenghts and incorporating a wide range of reactive aggregate types and natures. *Cement and Concrete Research*.
- Saouma, V., & Perotti, L. (2006). Constitutive model for alkali-aggregate reactions. *ACI materials journal*.
- Schlune, H., Plos, M., & Gylltoft, K. (2012). Safety formats for non-linear analysis of concrete structures. *Magazine of Concrete Research*, 563-574.
- Schmidt, J. W., Hansen, S. G., Barbosa, R. A., & Henriksen, A. (2014). Novel shear capacity testing of ASR damaged full scale concrete bridge. *Engineering Structures*.
- Senturk, M., Pul, S., Ilki, A., & Hajirasouliha, I. (2020). Development of a monolithic-like precast beam-column moment connection: Experimental and analytical investigation. *Engineering Structures*, 110057.
- Shima, H., Chou, L.-L., & Okamura, H. (1987). Micro and Macro Models for Bond in Reinforced Concrete. *Journal of the Faculty of Engineering, The University of Tokyo*, 132-193.
- Shirzehhagh, M., & Fakhimi, A. (2021). Insights on crack initiation and propagation in reinforced concrete beams, a bonded-particle approach. *Engineering Structures*, 112783.
- Simo, J., & Ju, J. (1987). Strain- and stress-based continuum damage models—I. Formulation. *International Journal of Solids and Structures*, 821-840.

- Sims, I., & Pool, A. B. (n.d.). *Alkali-Aggregate Reaction in Concrete: A world Review*. 2017: CRC Press.
- Slowik, O., Novák, D., Novák, L., & Strauss, A. (2021). Stochastic modelling and assessment of long-span precast prestressed concrete elements failing in shear. *Engineering Structures*, 111500.
- Smaoui, N., Berube, M. A., Fournier, B., Bissonnette, B., & Durant, B. (2004). Evaluation of the expansion attained to date by concrete affected by alkali-silica reaction. Part I: Experimental study. *Canadian Journal of Civil Engineering*.
- Smaoui, N., Bérubé, M., Fournier, B., & Bissonnette, B. (2004). Influence of specimen geometry, orientation of casting plane, and mode of concrete consolidation on expansion due to ASR. *Cement, Concrete, and Aggregates*.
- Smaoui, N., Bissonnette, B., Bérubé, M. A., Fournier, B., & Durand, B. (2005). Mechanical properties of ASR-affected concrete containing fine or coarse reactive aggregates. *Journal of ASTM International*.
- Srivaranun, S., Akiyama, M., Bocchini, P., Christou, V., Fukushima, D. M., & Masuda, K. (2021). Effect of the interaction of corrosion pits among multiple tensile rebars on the reliability of RC structures: Experimental and numerical investigation. *Structural Safety*, 102115.
- Stemland, K., Johansen, H., & Kanstad, T. (2023). Load Effects of ASR-induced Expansion in Reinforced Concrete and Their Consequences for Structural Assessment. *NCR Journal*, 68, 39-63.
- Stemland, K., Rodum, E., & Kanstad, T. (2022). Stiffness damage testing of laboratory-cast alkali-silica reactive concrete and cores drilled from an existing concrete structure. *16th International Conference on Alkali-Aggregate Reaction in Concrete (ICAAAR)*. Lisbon, Portugal.
- Stramandinoli, R. S., & Rovere, H. L. (2008). An efficient tension-stiffening model for nonlinear analysis of reinforced concrete members. *Engineering Structures*, 30(7), 2069-2080.
doi:doi:10.1016/j.engstruct.2007.12.022
- Sun, P., & Zhu, H. (2021). Numerical simulation of fracturing behavior of reinforced concrete structures using independent cover method. *Engineering Failure Analysis*, 105559.
- Swamy, R. N., & Al-Asali, M. M. (1988). Engineering properties of concrete affected by alkali-silica reaction. *Materials Journal*.
- Tan, R., Hendriks, M., Geiker, M., & Kanstad, T. (2019). Modified cracked membrane model for consistent crack width predictions of reinforced concrete structures subjected to in-plane loading. *Engineering Structures*. doi:https://doi.org/10.1016/j.engstruct.2019.109362
- Tao, J., Ren, X., & Chen, J. (2021). Random transition of failure modes in concrete shear walls with constitutive parameters involving spatial variation. *Engineering Structures*, 112508.
- Taresh, H., Yatim, M., & Azmi, M. (2021). Punching shear behaviour of interior slab-column connections strengthened by steel angle plates. *Engineering Structures*, 112246.
- Terán, J. D., & Haach, V. G. (2018). Equivalent stress-strain law for embedded reinforcements considering bond-slip effects. *Engineering Structures*, 247-253.
- Terán, J. R., & Haach, V. G. (2018). Equivalent stress-strain law for embedded reinforcements considering bond-slip effects. *Engineering Structures*, 247-253.
- Ulm, F., Coussy, O., Kefei, L., & Larive, C. (2000). Thermo-chemo-mechanics of ASR expansion in concrete structures. *Journal of engineering mechanics*.
- Vecchio, F. J., & Collins, M. P. (1986). MODIFIED COMPRESSION-FIELD THEORY FOR REINFORCED CONCRETE ELEMENTS SUBJECTED TO SHEAR. *Journal of the American Concrete Institute*, 219-231.
- Vermeer, P., & Borst, R. d. (1984). Non-associated plasticity for soils, concrete and rock. *HERON*.
- Wald, D., Allford, M., Bayrak, O., & Hrynkyk, T. (2017). Development and multiaxial distribution of expansions in reinforced concrete elements affected by alkali-silica reaction. *Structural Concrete*.
- Wang, D.-b., Song, X.-b., & Nie, H.-y. (2022). Cracking analysis of massive concrete with large-diameter pipes during construction. *Construction and Building Materials*, 127636.
- Wang, Q., Le, J.-L., & Ren, X. (2022). Numerical modeling of delayed damage and failure of concrete structures under sustained loading. *Engineering Structures*, 113568.
- Wang, Y., Pan, Z., Zhao, C., & Zeng, B. (2023). Long-term behavior of prestressed concrete industrial buildings in chloride-based industrial environments. *Journal of Building Engineering*, 107344.

- Wang, Z., Gong, F., Zhang, D., Wang, Y., & Ueda, T. (2019). RBSM based analysis on mechanical degradation of non-air entrained concrete under frost action – A general prediction with various water cement ratio, lowest temperatures and FTC numbers. *Construction and Building Materials*, 744-755.
- Wang, Z., Hayashida, H., Zhang, D., Gong, F., & Ueda, T. (2020). Structural behaviors evaluation of RC beam under frost damage – A methodology with meso-macro material/bond simulation and integrating into structural analysis. *Engineering Structures*, 110162.
- Wani, F. M., Khan, M. A., & Vemuri, J. (2022). 2D nonlinear finite element analysis of reinforced concrete beams using total strain crack model. *Materials Today: Proceedings*, 1305-1313.
- Wani, F., Khan, M. A., & Vemuri, J. (2022). 2D nonlinear finite element analysis of reinforced concrete beams using total strain crack model. *Materials Today: Proceedings*, 1305-1313.
- Wen, H. (1993). Prediction of structural effects in concrete affected by alkali-aggregate reaction. *PhD Thesis*.
- WILLAM, K., & WARNKE, E. P. (1975). Constitutive Model for the Triaxial Behaviour of Concrete. *Constitutive Model for the Triaxial Behavior of Concrete, Proceedings of IABSE, Structural Engineering*, 1-30.
- Xi, X., S. Yang, & Li, C.-Q. (2018). A non-uniform corrosion model and meso-scale fracture modelling of concrete. *Cement and Concrete Research*, 87-102.
- Yang, J., Wang, L., Yang, D., & Wang, Q. (2023). Influence of concrete and unbonded ratio on RC beams. *Construction and Building Materials*, 133086.
- Yang, S., Li, K., & Li, C. (2018). Numerical determination of concrete crack width for corrosion-affected concrete structures. *Computers & Structures*, 75-82.
- Yoshitake, I. W. (2013). *Yoshitake, Isamu, Wenbo Zhang, Yoichi Mimurac and Tadashi Saito (2013): Uniaxial tensile strength and tensile Young's modulus of fly-ash concrete at early age*. *Construction and Building Materials* 40 (2013) 514-521.
- Yu, Q., Ruiz, M. F., & Muttoni, A. (2022). Considerations on the partial safety factor format for reinforced concrete structures accounting for multiple failure modes. *Engineering Structures*, 114442.
- Zahedi, A., Trottier, C., Sanchez, L., & Noël, M. (2022). Evaluation of the induced mechanical deterioration of alkali-silica reaction affected concrete under distinct confinement conditions through the Stiffness Damage Test. *Cement and Concrete Composites*.
- Zhang, Q., & Wang, L. (2021). Investigation of stress level on fatigue performance of plain concrete based on energy dissipation method. *Construction and Building Materials*, 121287.
- Zhao, M.-Z., Lehman, D. E., & Roeder, C. W. (2021). Modeling recommendations for RC and CFST sections in LS-Dyna including bond slip. *Engineering Structures*, 111612.
- Zhong, J., Zhuang, H., Shiyang, P., & Zhou, M. (2021). Experimental and numerical analysis of crack propagation in reinforced concrete structures using a three-phase concrete model. *Structures*, 1705-1714.
- Zhu, J., & Ren, X. (2022). Failure modeling of concrete: A peri-dynamical approach with bond-based correspondence to bi-scalar damage model. *Engineering Fracture Mechanics*, 108470.

EXCON

<https://sintef/excon>



Prosjektet er finansiert av Grønn Plattform ordningen som er et samarbeid mellom Forskningsrådet, Innovasjon Norge, Siva og Enova, og følgende deltagere:

